ELECTRODEPOSITION OF ZnO THIN FILMS: EFFECT OF VANADIUM DOPING

A THESIS SUBMITTED TO
THE GRADUATE SCHOOL OF NATURAL AND APPLIED SCIENCES
OF
MIDDLE EAST TECHNICAL UNIVERSITY

BY

CEMRE AVŞAR

IN PARTIAL FULFILLMENT OF THE REQUIREMENTS
FOR
THE DEGREE OF MASTER OF SCIENCE
IN
CHEMICAL ENGINEERING

SEPTEMBER 2013

Approval of the thesis:

ELECTRODEPOSITION OF ZnO THIN FILMS: EFFECT OF VANADIUM DOPING

submitted by **CEMRE AVŞAR** in partial fulfillment of the requirements for the degree of **Master of Science in Chemical Engineering Department, Middle East Technical University** by,

Prof. Dr. Canan Özgen _____
Dean, Graduate School of **Natural and Applied Sciences**

Prof. Dr. Deniz Üner _____
Head of Department, **Chemical Engineering**

Prof. Dr. Gürkan Karakaş _____
Supervisor, **Chemical Engineering Dept., METU**

Examining Committee Members:

Prof. Dr. Hayrettin Yücel _____
Chemical Engineering Dept., METU

Prof. Dr. Gürkan Karakaş _____
Chemical Engineering Dept., METU

Assoc. Prof. Dr. Ayşen Yılmaz _____
Chemistry Dept., METU

Assoc. Prof. Dr. Meltem Ünal Doğan . _____
Chemical Engineering Dept., Gazi University

Dr. Alp Yürüm _____
Nanotechnology Research and Application Center, Sabancı University

Date: **03.09.2013**

I hereby declare that all information in this document has been obtained and presented in accordance with academic rules and ethical conduct. I also declare that, as required by these rules and conduct, I have fully cited and referenced all material and results that are not original to this work.

Name, Last name : CEMRE AVŞAR

Signature :

ABSTRACT

ELECTRODEPOSITION OF ZnO THIN FILMS: EFFECT OF VANADIUM DOPING

Avşar, Cemre

M. Sc., Department of Chemical Engineering

Supervisor: Prof. Dr. Gürkan Karakaş

September 2013, 86 Pages

The aim of this study was preparation and characterization of photocatalytically active ZnO thin films on ITO glass sheets by electrodeposition method. In order to investigate the effect of synthesis temperature on the morphology and photocatalytic activity of the thin films, synthesis was performed at room temperature and at 70 °C. Characterizaton of the thin films was carried out by AFM, SEM - EDX, XRD and XPS analysis. Photocatalytic activity of the samples was tested by methylene blue and stearic acid degradation tests. Methylene blue degradation tests were examined by obtaining the absorbance data between 200-800 nm by UV- Vis spectrophotometer. Stearic acid degradation tests were examined by monitoring the difference in the asymmetric C-H streching modes of CH_3 groups and the symmetric- asymmetric C-H streching modes of CH_2 groups in the region 2700-3000 cm^{-1} by FT- IR spectrophotometer. ZnO thin films were dip coated with a transition metal, vanadium, in order to investigate the effect of vanadium doping on the photocatalytic activity of thin films. Dip coating was performed with NH_4VO_3 solutions, in which NH_4VO_3 was dissolved in water and oxalic acid and vanadium was existing in (+5) and (+4) oxidation states, respectively.

Photocatalytic activity tests performed by the degradation of methylene blue and stearic acid on both vanadium doped and undoped ZnO thin films synthesized at room temperature and 70 °C indicated that the photocatalytic activity of thin films had been improved by vanadium doping and it was also favored by the synthesis temperature. It was observed from SEM images that, vanadium was not homogenously dispersed on the surface of the thin films. SEM images also showed the effect of synthesis temperature on the morphology of the ZnO thin films. The oxidation state of vanadium was determined by XPS analysis.

Keywords: Zinc oxide, thin film, electrodeposition, photocatalysis

ÖZ

ÇİNKO OKSİT İNCE FİLMLERİN ELEKTRODEPOZİSYONU: VANADYUM KATKILAMANIN ETKİSİ

Avşar, Cemre

Yüksek Lisans, Kimya Mühendisliği Bölümü

Tez Yöneticisi: Prof. Dr. Gürkan Karakaş

Eylül 2013, 86 Sayfa

Çalışmanın amacı, fotokatalitik olarak aktif çinko oksit filmlerin elektrodepozisyon metodu ile hazırlanması ve karakterizasyonudur. Sentez sıcaklığının filmlerin morfolojisi ve fotokatalitik aktiviteleri üzerindeki etkisini incelemek amacıyla filmlerin sentezi oda sıcaklığında ve 70 °C 'de yapılmıştır. Filmlerin karakterizasyonu AFM, SEM. EDX, XRD ve XPS yöntemleriyle yapılmıştır. Fotokatalitik aktivite testleri metilen mavisi ve steraik asit bozulma reaksiyonları ile gerçekleştirilmiştir. Metilen mavisi bozulması, UV-Vis spektrofotometre kullanılarak 200- 800 nm dalga boyu arasında alınan absorbans verileri ile incelenmiştir. Stearik asit bozulması ise FT-IR spektrofotometresi kullanılarak 2700- 3000 cm^{-1} bölgesindeki CH_3 ve CH_2 gruplarına ait C-H bağlarının değişimi ile incelenmiştir. Hazırlanan çinko oksit ince filmler vanadyum ile katkılama yapılmış ve vanadyumun filmlerin fotokatalitik aktivitesi üzerindeki etkisi incelenmiştir. Vanadyum katkılama işlemi amonyum metavanadatın sulu ve okzalik asitteki çözeltileri ile gerçekleştirilmiştir. Vanadyumun oksitlenme sayısı ilk çözeltide (+5), ikinci çözeltide de (+4) olarak belirlenmiştir.

Fotokatalitik aktivite testleri hem oda sıcaklığında hem 70 °C'de hazırlanmış, vanadyum ile katkılama yapılmış ve yapılmamış örneklerle gerçekleştirilmiştir. Test sonuçları, ince filmlerin fotokatalitik aktivitesinin vanadyum katkılaması ve sıcaklıkla arttığını göstermiştir. SEM görüntüleri, vanadyumun film yüzeylerine homojen olarak dağılmadığını göstermiştir. Sentez sıcaklığının çinko oksit ince filmlerin morfolojisi üzerindeki etkisi de SEM görüntüleri ile gözlemlenmiştir. Vanadyumun oksitlenme sayısı ise XPS analizi ile belirlenmiştir.

Anahtar Kelimeler: Çinko oksit, ince film, elektrodepozisyon, fotokataliz.

To My Parents…

ACKNOWLEDGEMENTS

I would firstly thank my supervisor, Prof. Dr. Gürkan Karakaş for his valuable academic guidance and encouraging support throughout this study. It was an honor for me to work with him during my MSc education.

It was a wonderful chance for me to assist Prof. Dr. Canan Özgen in Introduction to Chemical Engineering and Process Control courses. I have learnt and will be learning much from her.

I am especially thankful to Kerime Güney for her wonderful smile and never ending support during my laboratory days.

I also want to thank especially to Ekin Karakaya for her valuable friendship, not knowing each other during our undergraduate education is really a big lost for us.

I will also remember Selin Noyan, Burçin İkizer, Seval Gündüz, S. Gökçe Avcıoğlu and Özgen Yalçın for giving small coffee breaks during experiments, Erdem Balık for creating toluene scented atmosphere in the laboratory and Serdar Asmaoğlu for his partnership in the laboratory during long term experiments all summer long.

I am also pleased to my group members Tuğçe Kırbaş and Birsu Aydoğdu for their friendship and support.

My valuable friends Gülşah Arslan, Serdar Surat, Safa Ercan, Melis Özbay Güney, Kamil Akyıldız, Gözde Ermetal Karadeniz, Doğaç Çağıl, Fatih Peker, Özge Süfer and Özge Çelikkol. I am grateful for all of your very valuable friendship during seven years.

I would like to express my deepest thanks to my lovely family. I firstly present my sincere gratitude to my lovely father, Prof. Dr. Dursun Avşar. Without him, I would probably not adopt being an academician as a profession. I am also thankful to my lovely mother, Zübeyde Avşar for her support, encouragement and endless love. Finally, my very very precious sister Ayşegül Avşar Tuncay and my brother-in-law Baki Tuncay; I could not find a word to express my feelings to this wonderful couple but it is, sure, more than “thank you”.

TABLE OF CONTENTS

LIST OF TABLES

LIST OF FIGURES

CHAPTER 1

INTRODUCTION

Materials are classified into three groups as conductors, semiconductors and insulators according to their electrical properties. Electrical conductivity of conductors have the highest value, on the other hand, insulators have very low electrical conductivity. Electrical conductivity value of semiconductors are between to those of conductors and insulators [1]. The conductivity of semiconductors can be enhanced by thermal excitation of electrons, which means that the conductivity in semiconductors is directly proportional to the temperature. Addition of impurity atoms results an increase of the number of atoms in the conduction band [2,3].

Electronic characteristics of materials are described by the "Band Theory" [4]. Energy levels of each band in a solid material are different and they are filled with electrons from the lowest energy to the highest one. Band gap is defined as the energy gap separating the valence and conduction bands and they are classified as direct and indirect band gaps. Direct band gap corresponds to the equal momentums of the electrons and holes at valence and conduction bands and electrons can emit phonons. If the maximum energy of the valence band is observed at the different value of momentum to the minimum in the conduction band energy, the semiconductor demonstrate indirect band gap. In this case, electrons and holes have different momentum [5].

Semiconductors are widely used in the production of electronic components, anti-static coatings, touch- screen LCD monitors, gas sensors, optical filters. Semiconductor metal oxides are widely used in light filtering and self cleaning applications, solid state gas sensors, and photocatalysts. Photocatalysis can be defined as the process, where light is used in order to activate the photocatalyt. ZnO, TiO_2, Fe_2O_3, CdS and ZnS are the commonly known semiconductors and they can be used as the sensitizers for light reduced redox processes. Heterogenous photocatalysis is intensively studied about environmental applications, mostly for energy renewal and energy storage areas, especially for the water splitting processes in order to produce hydrogen gas and for the total purification of polluted air and water from organic compounds [6- 10]. Metal oxide semiconductors are extensively used as photocatalysts. They are appropiate for photocatalytic applications due to their wide band gap energies, having suitable band gap energy conditions for supplying reductive and oxidative processes and their photocorrosion resistance. Semiconductors are extensively used as photocatalysts but the most commonly used semiconductors for this purpose are TiO_2 and ZnO. Performance of a photocatalytic reaction can be affected by the type of pollutant to be degraded, type of the photocatalyst, concentration of the pollutant and the photocatalyst, the

intensity of light irradiation and the wavelength. It has also been reported that, the structural and morphological properties and the synthesis method aslo affect the photocatalytic activity. The photocatalytic activity can be improved by doping, dye sensitizing and semiconductor coupling [11, 20].

Photocatalysts are widely used as powder samples in most of their applications, resulting a difficulty in separation processes and decrease in the photon efficiency. In order to avoid the difficulties in separation processes and the decrease in photon efficiency, photocatalysts should be used as thin film samples.

Zinc Oxide is a semiconductor metal oxide having a band gap energy of 3.37 eV and an exciton binding energy of 60 meV [21]. Zinc oxide is electrochemically active, chemically stable and its thermal conductivity has a high value, an appropiate material for optoelectronic, spintronic and pigment applications and is non-toxic to human body [22, 24]. ZnO shares three types of crystal structures which are wurtzite, rocksalt and zinc blende [25].

Similar to other semiconductor metal oxides, zinc oxide nanostructured thin films can be grown by vacuum deposition techniques such as chemical vapor deposition (CVD), metal organic chemical vapor deposition (MOCVD), carbothermal method, plasma enhanced chemical vapor deposition, pulsed laser deposition, molecular beam epitaxy, sputtering. On the other hand, electrochemical deposition and electrophoresis which have some advantages such as lower equipment cost, easy to apply, does not require high temperatures and the film thickness can be controlled easily by adjusting the temperature or applied potential [26, 36].

In this study, ZnO thin films were synthesized on ITO glass sheets by electrodeposition method. The effect of synthesis temperature on the structure and the photocatalytic activity of zinc oxide thin films were studied. Vanadium doping was performed in order to observe the effect of vanadium doping on the photocatalytic activity of electrodeposited zinc oxide thin films. Characterization of thin film samples was perfomed with UV- Vis, AFM, SEM, XRD and XPS. Photocatalytic activity of the thin film samples was examined by methylene blue and stearic acid degratation tests.

CHAPTER 2

LITERATURE SURVEY

2.1. Semiconductors

Materials are classified into three groups as conductors, semiconductors and insulators according to their electrical conductivity. Conductors have the highest electrical conductivity, with a value of 10^{7} $(\Omega m)^{-1}$, whereas insulators have very low electrical conductivity, 10^{-10} $(\Omega m)^{-1}$. Semiconductors have the electrical conductivity value between $10^{-6} – 10^{4}$ $(\Omega m)^{-1}$[5].

Conduction band is overlapped by the valence band in conductors and electrons can freely move across all atoms in the solid and they can have an access to the empty holes within the valence band [4].The electrical resistivity of conductors has a very low value. When an electric field is applied, the electrons at the top of the valence band gain kinetic energy and thus they can easily move to the next higher available energy level. In conductors, valence electrons can freely move in the conduction band [2].

On the contrary, the valence band and the conduction band are seperated by a large gap in insulators. Their valence band is occupied by electrons, whereas the energy levels in conduction band are all empty. The band gap value in insulators have large values. This means that the distance between the valence band and the conduction band is large in terms of energy to be accessed by the electrons. Strong bonds, which are difficult to be broken, are formed between the valence electrons and neighboring atoms.

Semiconductors are known as the materials which have an electrical conductance between that of an electrical conductor and an electrical insulator. Band gap values in semiconductors are small enough for electrons to be upgraded from the valence band to the conduction band by the effect of heat or light. The conductivity of semiconductors can be enhanced by thermal excitation of electrons, which means that the conductivity in semiconductors is directly proportional to the temperature. The energy of photons upgrade the electrons from valence band to conduction band in semiconductors [2]. . Schematic representation of the valence and conduction band positions for some of the semiconductors are given in figure 2.1. below.

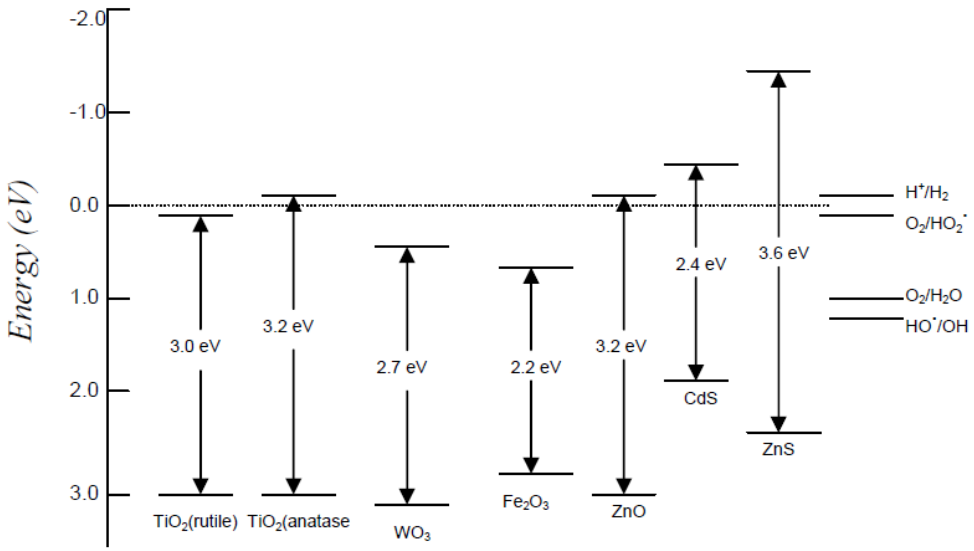

Figure 2.1. Valence and conduction band positions for some of the semiconductors [8]

Band gap (E_{bg}) is the energy gap which seperates the valence and conduction bands. Band gap of materials can be classified as direct band gap and indirect band gap. The momentum of electrons and holes at valence and conduction bands are equal to each other for a direct band gap. Electrons can easily be excited to the conduction band by absorbing a photon. Indirect band gap term is defined as the band gap when the momentum of the electrons and holes at valence and conduction bands are not equal to each other. In addition to a photon, additional energy corresponding to the difference in the momentum of the valence band electrons and holes is also necessary to excite valence band elecrons of indirect band gap material. Crystal lattice energy can be the source of this momentum change. A phonon is described as the vibration energy of atoms in the crystal. Absorption or emission of phonons can cause the momentum change which is needed for the excitaton of the electron in an indirect band structure [5]. Direct and indiect band gap structures are depicted in figure 2.2..

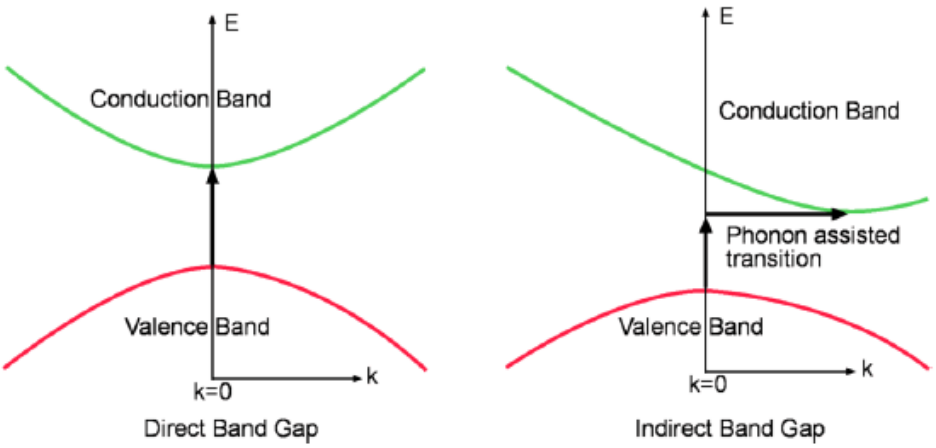

Figure 2.2. Direct and indirect band gap structures [5]

Semiconductors can be generally classified as *Intrinsic* or *extrinsic* semiconductors. Si, Ge, InSb, GaAs, SiC semiconductors can be given as an example for Intrinsic semiconductors. Intrinsic semiconductors possess low conductivity at room temperature and they do not have any charge carriers at the temperature of absolute zero, resulting to behave as an insulator. Their valence band is completely filled with electrons and the conduction band is empty. If a valence band electron is excited, it leaves an unoccupied state in the valence band and promotes to the conduction band. This unoccupied state is called as a *hole* (h^+). There is a corresponding empty state in the valence band for each of the electrons in the conduction band in Intrinsic semiconductors, thus electron and hole concentration are equal to each other. This concentration is called as the *Intrinsic carrier concentration* (n_i) [4].

The conductivity of the semiconductor material can be enhanced by the addition of impurity atoms, resulting the increase of the number of the electrons in the conduction band [3]. Extrinsic semiconductors can be formed by introduction of acceptor sites to the valence band or introduction of donor sites to the conduction band [37]. Schematic representations of extrinsic semiconductors for both of the acceptor and donor sites are illustrated in figure 2.3.

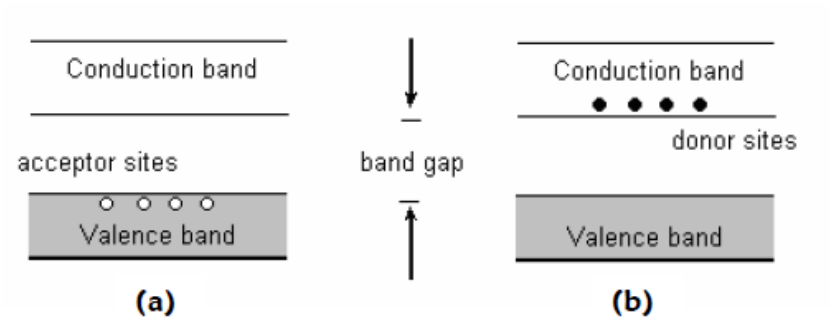

Figure 2.3. Energy band representation of extrinsic semiconductors with acceptor sites (a) and donor sites (b) [2]

Donors are the chemical impurities that contribute the conduction electrons. When a semiconductor is doped with a donor, it conducts with the negatively charged free electrons and the semiconductor formed by this type of doping is called as *n- type semiconductors* [38]. Electrons are the majority and holes are the minority carriers in n- type semicondcutors. Electron concentration, n, is equal to the donor impurity concentration [4].

Acceptors are the impurity atoms which take an electron away from a semiconductor. When a semiconductor is doped with an acceptor, it conducts with the positively charged holes moving through the structure and the semiconductor formed by this type of doping is called as *p- type semiconductors.* The prefixes *n* and *p* represents negative and positive, respectively [38]. Holes are the majority and electrons are the minority carriers in p- type semiconductors and p is equal to the acceptor impurity concentration [4]. Band gap structures of n- type and p- type semiconductors are given in figure 2.4. below.

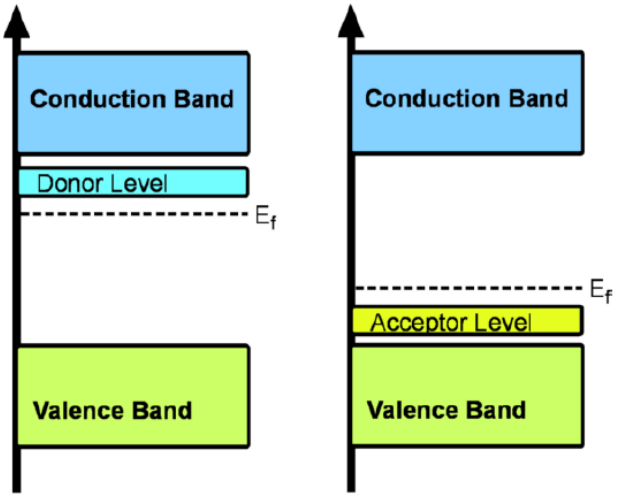

Figure 2.4. Band gap structures of n-type and p-type semiconductors [5]

Semiconductors are widely used in the production of anti-static coatings, touch- screen LCD monitors, gas sensors, optical filters and photocatalysts due to their electronic configuration.

ZnO nanoparticles are reported to show n- type semiconductor behaviour due to the native defects such as oxygen vacancies and Zn interstitials.

2.2. Zinc Oxide

Wide direct band gap value makes zinc oxide an appropiate material for optoelectronic applications, transparent conducting films and excitonic emission processes can occur near or above room temperature due to large exciton binding energy value of the material [22]. Except wide direct band gap and large exciton binding energy values, zinc oxide has gained interest because it is electrochemically active, chemically stable, has a high thermal conductivity and high electron mobility [21,23]. Ferromagnetic properties of zinc oxide allows this material to be applicable for spintronic applications, additionally zinc oxide is a useful material in pigment applications because of its high refractive index value [21].

Zinc oxide is a multi-functional material for the applications in UV- lasers, transparent electronics, piezoelectric and photovoltaic systems, photodetectors, dye sensitized solar cells, gas sensors, chemical sensors and biosensors [21]. Zinc oxide is an appropiate material for the production of small size devices since it is easily etched in acidic and alkali media and its resistance to high energy radiation allows zinc oxide to be used for space applications [25].

In addition, zinc oxide based nanostructures exhibit high biological activity in binding of biomolecules, which increases the sensing characteristics. Since zinc oxide is biocompatible, it is a potential material for integrated biosensor devices [21].

Zinc oxide is not carcinogenic or genotoxic material to human body, it is non-toxic. However, if necessary safety precautions are not taken, zinc powder may be hazardous by inhalation or ingestion. Although zinc oxide is non-toxic to human body, animals and plants and trace amounts of it is needed; soluble zinc compounds have toxic effects on aquatic organisms [24].

Zinc oxide can be produced by hydrometallurgical or pyrometallurgical methods such as spray pyrolysis, the direct and indirect processes [24]. The reason why the growth mechanism of zinc oxide thin films have been studied extensively in recent years is because they have perfect piezoelectric properties and they tend to grow on diverse substrates such as diamond, glass or sapphire [25].

2.2.1. Crystal Structure of Zinc Oxide

Zinc oxide is a II-VI compound semiconductor. Crystal structures of the most of the II- VI group semiconductors are in cubic zinc blende or hexagonal wurtzite form. Group II-VI semicondutors have a typical sp^3 covalent bonding but, they also show ionic character.

ZnO shares three types of crystal structures which are wurtzite, rocksalt and zinc blende [25]. Among these three crystal structures, wurtzite form is thermodynamically the most stable one under ambient conditions. Rocksalt structure can be stabilized only at higher pressures [24]. Cubic rocksalt, cubic zinc blende and hexagonal wurtzite structures of ZnO are represented in figure 2.5. below.

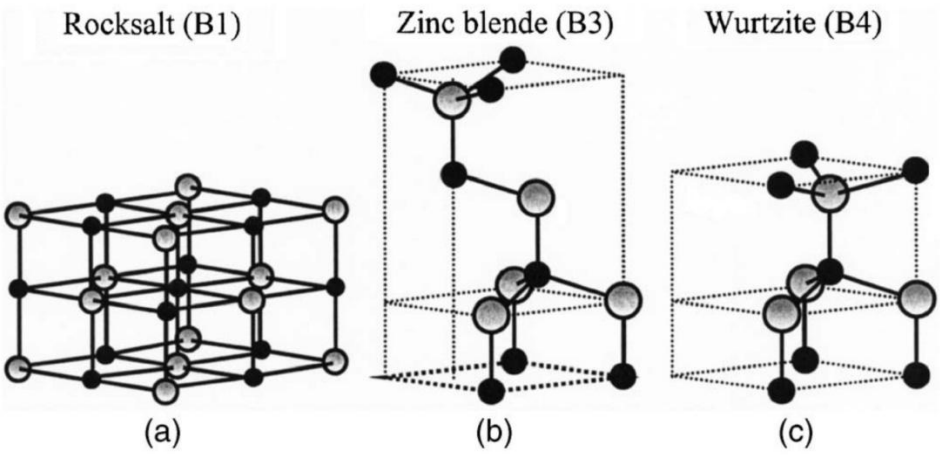

Figure 2.5. ;Crystal structures of ZnO; cubic rocksalt (a), cubic zinc blende (b), hexagonal wurtzite (c). (gray spheres represent zinc, black spheres represent oxygen atoms) [25]

2.2.2. Growth Methods of Zinc Oxide Nanoparticles

ZnO nanostructures can be grown by various methods and results with a variety of physical and chemical properties.

2.2.2.1. Vacuum Deposition Techniques

The most widely used growth methods for the fabrication of zinc oxide nanostructures is chemical vapor deposition (CVD). With this method, nanorods can be grown on different substrates without using any catalysts but it is observed that the optical properties of the obtained nanorods were dependent on the substrate used [26].

Carbothermal method is also a commonly used method for the growth of zinc oxide nanostructures. In this method, zinc oxide- carbon mixture is used as source material. Graphite is the most commonly used carbon source. High growth temperature requirement is a disadvantage but, nanostructures having different kinds of morphologies and different optical properties can be obtained by this method [26].

Metal organic chemical vapor deposition (MOCVD) is also a method for the growth, in which zinc oxide nanoparticles having different morphologies can be obtained due to Zn- and O- rich conditions. If the growth is carried out at low temperatures and Zn- rich conditions, obtained nanoparticles have smooth surfaces. However, if the growth is carried out at high temperatures and O- rich conditions, obtained nanoparticles have stacked- pyramid morphology. Growth under Zn- and O- rich conditions also affect the cathodoluminesence (CL) and photoluminesence (PL) spectra of zinc oxide nanoparticles [26].

Plasma-enhanced chemical vapor deposition method is carried out in two steps, which are nucleation and growth. Zinc oxide nanoparticles are grown without the use of catalysts in this method. Morphologies and the optical properties of the zinc oxide nanoparticles grown with plasma-enhanced chemical vapor deposition method are slightly affected by the substrate used. [26].

ZnO thin films can be prepared by pulsed laser deposition (PLD) method. Pulsed laser deposition is an available method, additionally, this method can be used for all kinds of oxides, nitrides, carbides, fullerenes, polymers and metallic systems [27]. In this method, deposition temperature inversely affects the growth rate of ZnO thin films, increase in the substrate temperature results a continous decrease in the growth rate of thin films. Highly crystalline zinc oxide thin films can be prepared by pulsed laser deposition method [28]. This method is a promising method for the growth of oxides, since deposition can be carried out rapidly under a high partial pressure of oxygen [29].

Molecular beam epitaxial growth of zinc oxide nanoparticles is a recently developed method when compared to CVD and PLD methods. In this method, the most important point for the preparation of zinc oxide thin films is the selection of the most appropiate substrate, since substrates have a crucial role since they generate active oxygen atoms. It has been reported that sapphire is an appropiate substrate for the growth of zinc oxide thin films by molecular beam epitaxy method. It has been reported that, a buffer layer grown initially on sapphire substrate or post treatment at higher temperatures under oxygen or nitrogen is necessary for the improvement of the crystallinity, morphology, optical and electrical properties of the resulting thin films [30].

Growth of zinc oxide thin films in relatively low temperatures is possible with sputtering method. High deposition rate is also an advantage of sputtering method. Structural and

morphological properties of the grown zinc oxide thin films are dependent on the synthesis conditions such as temperature, pressure and distance of substrates. Inert gases are also important in sputtering method because due to their high molecular weight, they produce higher deposition rates [30].

2.2.2.2. Solution- Growth Mechanisms

Solution- growth mechanisms are also used for the growth of zinc oxide nanoparticles. These methods can be classified into three groups; which are hydrothermal, solvothermal and electrochemical deposition (electrodeposition) methods.

The difference between hydrotermal and solvothermal method is the solvent used in the synthesis, hydrothermal method uses water as the solvent, whereas solvothermal method uses other solvents other than water [31]. The usage of hydrothermal method is more general when compared to solvothermal method, since zinc oxide nanoparticles can be grown at lower temperatures in aqueous solutions. Morphology and the optical properties of the zinc oxide nanoparticles synthesized by hydrothermal and solvothermal methods are affected by the reaction time, the concentration of the precursor, the surfactant, the solvent and the temperature. The collodial solutions of nanostructured zinc oxide can be employed to obtain powder samples as well as thin films by using dip coating, spray coating or electrophoretic coating.

2.2.2.3. Electrochemical Deposition (Electrodeposition)

Electrochemical deposition, also known as electrodeposition is an electrochemical method which uses aqueous solutions for the growth of zinc oxide nanoparticles [32]. Reagents used in electrodeposition are similar to those which are used in hydrothermal growth. When compared to hydrothermal growth, electrodeposition has higher growth rates [33]. Electrodeposition has some advantages among these methods. First of all, thin films having large surface area can be synthesized with low equipment costs [34]. Application of electrodeposition is simple, zinc oxide can be deposited at even low temperatures with this method and the control of the film thickness is also available [35]. The composition of the solution strongly affects the morphology of the resulting nanoparticles [26]. Ions (chloride, acetate and sulfate) also have effects on the morphology of the resulting nanoparticles due to the different OH^- generation rates [36].

Machado et al. studied the electrodeposition of indium doped ZnO thin film from aqueous $Zn(NO_3)_2$ solution, $InCl_3$ used as dopant. Electrodeposition was conducted at 80 °C and applid potential varied between 600- 800- 1000- 1200 mV [35]. Zhang et al. also studied the electrochemical properties of zinc oxide thin films obtained from a mixture of aqueous $Zn(NO_3)_2$ and KNO_3 solution. Concentration of $Zn(NO_3)_2$ solution varied between 0.01 to 0.1

M, whereas concentration of KNO_3 solution was constant, 0.1 M. Electrodeposition was conducted at 80 °C during 30 minutes and 1.3 VDC potential was applied. They reported the formation of ZnO films with grain sizes between 10 and 15 nm [34]. Mouet et al. studied the effect of concentration and applied potential on the growth mechanism of electrodeposited ZnO thin films in aquoues $ZnSO_4$ solution [32].Inamdar et al. studied the fabrication of nanocrystalline ZnO thin films bu using double pulse potentiostatic electrodeposition in zinc acetate bath onto FTO coated glass substrates [39]. Michaelis et. al studied electrodeposition of porous ZnO electrodes in the existence of SDS. Electrodeposition was performed in a mixture of 5 mM $ZnCl_2$ and 0.1 M KCl solution at 70 °C and 1 VDC potential was applied. Resulting ZnO thin films had large surface area and good porosity [40]. Yeo et al. used a 0.1 M $Zn(NO_3)_2$ solution as electrodeposition bath and performed electrodeposition at 65 °C [41]. Inamdar et al. also studied the growth mechanism of electrodeposited ZnO thin films. They used 50 nM zinc acetate and 0.1 M KCl solution as electrodeposition bath and performed electrodeposition at room temperature [42].

2.2.3. Properties of Zinc Oxide Nanoparticles

2.2.3.1. Optical Properties

Optical properties of zinc oxide are affected by the sytnthesis method and surface morphology of the particles [24].

Having a band gap energy of 3.37 eV at room temperature and a large exciton binding energy of 60 meV makes zinc oxide an appropiate material for the applications in optoelectronics in the blue/UV region [22].

Doping with different metal oxides increases or decreases the band gap energy of zinc oxide. Alloying with CdO and MgO results lower band gap and higher band gap materials, respectively [24].

Exciton binding energy is directly affected by quantum size confinement and it was reported that quantum size confinement causes a blue shift in the near UV emission peak in zinc oxide nanopatricles. Red luminesence spectra indicates the doubly ionized oxygen vacancies. Zinc oxide nanoparticles have large refractive indexes, which makes them promising materials for optical waveguides [43].

2.2.3.2. Mechanical, Electrical, Thermal and Magnetic Properties

The traditional mechanical behaviour measurement methods for bulk materials can not be applied on the individual nanostructures, as a result, direct measurement of the mechanical behaviour for nanostructures is challenging. The bending modulus of zinc oxide nanobelts is characterized using TEM. The method is an electric field induced resonant excitation. Results show that zinc oxide is an appropiate material as a nanoresonator and nanocantilever [43].

Zinc oxide nanostructures have been a subject of the studies in nanopiezotronics due to their mechanical and electromechanical properties. Nanopiezotronics deals with the piezoelectric nanostructures in order to accumulate energy in self- powered wireless nanodevices [23]. Piezoelectric effect in a cation- anion unit is represented in Figure 2.6, F and P denotes the applied force and polarization strength, respectively.

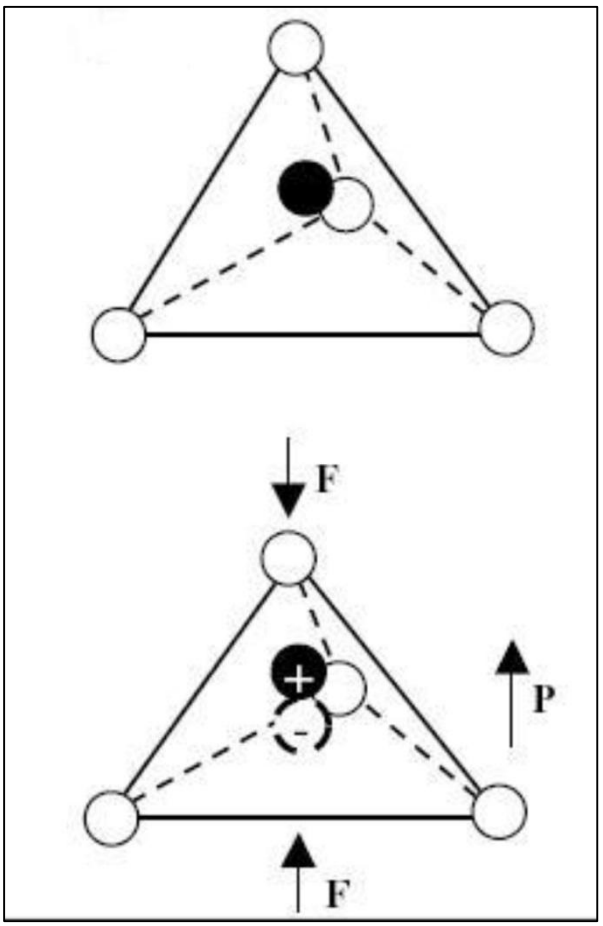

Figure 2.6. Representation of the piezoelectric effect in a cation- anion unit [43]

Electrical conductivity shows increase with increasing temperature in most of the semiconductors, and so of zinc oxide's. Electrical conductivity of zinc oxide is affected by its

stoichiometry because conductivity is dependent on the content of charge carriers. Stoichiometry can be adjusted by the partial pressures of oxygen and zinc during high temperature processes. Electrical conductivity is highly affected when zinc oxide is annealed in a reducing atmosphere with hydrogen. The conductivity of zinc oxide should be very high for the applications in which a transparent conducting oxide is used. B, Al, Ga or In are doping materials in order to increase the conductivity of zinc oxide. It is reported that In- doped zinc oxide nanomaterials show carrier concentrations around 10^{20} cm^{-3}, whereas undoped zinc oxide shows around 10^{15} cm^{-3} [24]. Electrically and chemically active oxygen vacancies are carried on metal oxide surfaces. These vacancies act as n- type donor, resulting an increase in the conductivity of the oxide [43].

Specific heat capacity and thermal conductivity of zinc oxide is reported to be relatively high, with a value of $40JK^{-1}mol^{-1}$ and 50 $WK^{-1}m^{-1}$, respectively [44]. Thermal conductivity of zinc oxide shows a decrease with the increase in the temperature or porosity. Expansion coefficient of zinc oxide has a value between 3 and $8x10^{-6}$ K^{-1} and is directly proportional to the increase in the temperature or porosity [6]

Crystalline zinc oxide shows thermochromic properties. When the temperature increases above 300 °C, zinc oxide changes from white to yellow and from yellow to white when cooling. Thermochromic behaviour of zinc oxide is probably a result of the formation of crystal lattice defects due to the loss of oxygen and the formation of non- stoichiometric $Zn_{(1+x)}O$. In this chemical formula, x is directly proportional with the temperature, shows an increase with the increase in the temperature [7]

2.3. Semiconductor Photocatalysis

The word *photocatalysis* has Greek origin and it is composed of two parts: *phos* and *katalyo*. The prefix *phos* means *light* in English and *katalyo* has a meaning of *decompose* or *brake apart*.

Photocatalysis term can be described as a process, where light is used in order to activate the photocatalyst. Here, photocatalyst is the substance which modifies the rate of the chemical reaction without being involved in it. The difference between a thermal catalyst and a photocatalyst is based on the type of energy by which they are activated. A conventional thermal photocatalyst is activated by heat, whereas a photocatalyst is activated by photons [4]. ZnO, TiO_2, Fe_2O_3, CdS and ZnS are the commonly known semiconductors and they can be used as the sensitizers for light reduced redox processes due to their electronic structure. The photoelectrochemical mechanism is explained in Figure 2.7 below.

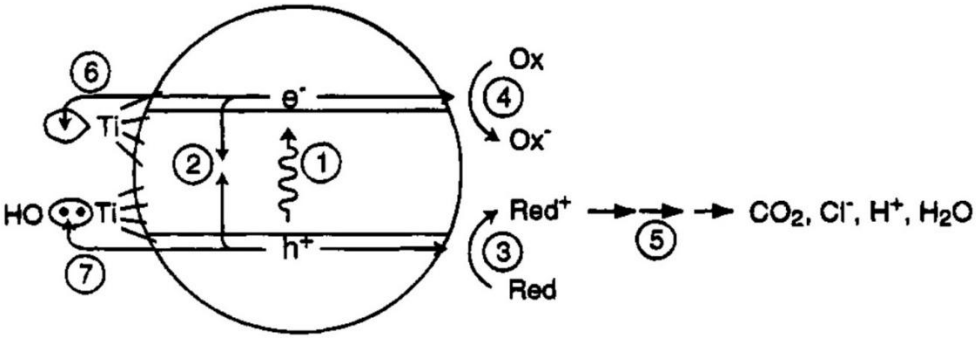

Figure 2.7. Representation of photoelectron mechanism [9]

First step is the formation of charge carriers by a photon absorption. This step is followed by the recombination of charge carriers in order to liberate heat. In third step, an oxidative pathway is initiated by a valence- band hole and this step is followed by the initiation of a reductive pathway by a conduction band electron.

When the bandgap (E_{bg}) of a semiconductor is matched or exceeded by a photon having an energy of $h\nu$, an excited valence band electron (e^-) is promoted to the conduction band, leaving hole (h^+) in the valence band. For a photocatalytic reaction, these excited electron and hole pairs can be directly used.

Most of the photocatalytic materials require high energy photons. Band gap energies and corresponding wavelengths of commonly used semiconductor metal oxides are given in Table 2.1

Table 2.1: Band gap energies and corresponding radiation wavelengths of commonly used semiconductors [8]

Semiconductor	Band gap Energy (eV)	Wavelength (nm)
TiO_2 (rutile)	3.0	413
TiO_2 (anatase)	3.2	388
ZnO	3.2	388
ZnS	3.6	335
CdS	2.4	516
Fe_2O_3	2.3	539
WO_3	2.8	443

The discovery of photocatalytic water splitting in 1972 and antibacterial effects of photocatalyti materials in 1985 initiated the extensive research area in catalysis field.

Heterogenous photocatalysis is intensively studied about environmental applications, mostly for energy renewal and energy storage areas, especially for the water splitting process in order to produce hydrogen gas and for the total purification of polluted air and water from organic compunds. Researches have shown that photocatalysis is also useful for the inactivation of cancer cells, odor control and the destruction of bacteria and viruses [9].

Reactions and photo- induced molecular transformations take place at the surface of the catalyst in a heterogenous photocatalysis system. Initial photoexcitation can occur either in an adsorbate molecule or in the catalyst substrate. The former case is called as a *catalyzed photoreaction*, where the initial photoexcitation occurs in the adsorbate molecule and than interacts with the ground state catalyst substrate. The latter case is called as a *sensitized photoreaction*, where the initial excitation occurs in the catalyst substrate and electron or energy is transferred into a ground state molecule by the photoexcited photocatalyst [10]. Electron or energy transfer occurs after the initial photoexcitation. Different interactions between a reactive center in the excited state and another reactive center in the ground state is illustrated in figure 2.8 by the electronic population changes in the molecular orbitals; A and D refer to acceptor and donor, respectively.

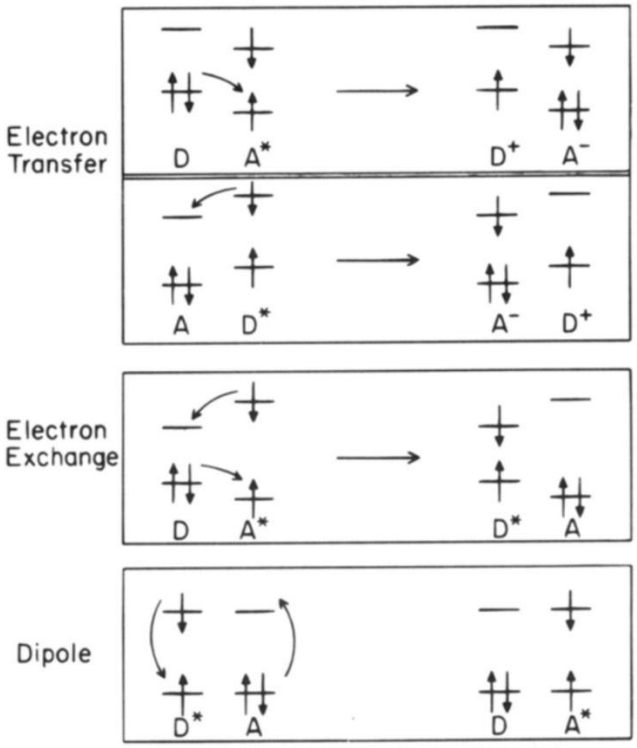

Figure 2.8. Electron transfer and energy transfer processes [10]

In an electron transfer process, the electron moves from an occupied orbital of the donor reactant to the vacant orbital of the acceptor reactant. Either the donor molecule or the acceptor molecule can be initially excited and an ion pair consisting of the donor cation (D^+) and

acceptor anion (A^-) occurs after the process. Electron exchange or dipole- dipole resonant coupling mechanisms occur in an energy transfer process, driving two fundamentally different mechanisms. Basically, an electron exchange process is the transfer of two independent electrons, transferred into each direction.

An orbital overlap is required for both of the electron transfer and electron exchange processes between the interacting centers. Electron transfer process would predominate in case of being thermodynamically available for both of these processes, since electron exchange process requires simultaneous overlap of two orbital pairs, whereas electron transfer process requires just one overlap [10].

2.4. Performance of the Photocatalytic Reactions

The efficiency of a photocatalytic reaction can be described as the effectiveness of the photons on the generation of free radicals [8]. Quantum efficiency or photon efficiency is used to benchmark the performance of photocatalysts.

Quantum efficiency is described as the ratio of photons used in the photocatalytic reactions to photons reaching to the photocatalyst surface. The calculation of quantum efficiency can be done by dividing the number of produced radicals to the number of absorbed photons [5].

The ratio of surface atoms to bulk atoms can be increased by decreasing particle size, increasing the surface area and the porosity of the catalyst. Surface to volume ratio increases with decreasing size and the effect of the surface becomes more important. Surface defects are also important in photocatalysis, since they can treat as hole traps [5].

The rate of the photocatalytic reaction is also affected by the adsorption of the reactants to the surface of the photocatalyst. The catalyst surface carries electron and hole pairs and the adsorbed reactants might react with the electrons, holes can reach the surface of the photocatalyst without recombining. Additionally, there might be decomposition risk for holes.

Increase in the surface area and porosity can increase the rate of adsorption on the catalyst surface. Modification of the surface morphology can also increase the adsorption rate. Other factors effecting the reaction efficiency can be listed as defects in the crystal structure, particle size distribution, impurities, acidity of the surface, hydrophobicity, electron- hole recombination and crystal phases [8].

2.5. Semiconductors as Photocatalysts

A good semiconductor photocatalyst should have properties like photo-activity and photo-stability. Additionally, they should be inert and inexpensive [11].

Semiconductors having low band gap energies are not suitable for photocatalytic applications. Having a low band gap energy means that, they need irradiation with low energy light. Metal oxide semiconductors are extensively used as photocatalysts. They are appropiate for photocatalytic applications due to their wide band gap energies, having suitable band gap energy conditions for supplying reductive and oxidative processes and their photocorrosion resitance [8].

Semiconductors are extensively used as photocatalysts but the most commonly used semiconductors for this purpose are TiO_2 and ZnO [12].

TiO_2 is the most available semiconductor metal oxide. Availability, chemical stability, biocompatibility, nontoxicity, physical, optical and electronic properties makes TiO_2 the most commonly preferred semiconductor metal oxide for photocatalytic applications. TiO_2 is chemically stable, it is insoluble in water and its band gap energy is available enough to provide reductive and oxidative processes. TiO_2 is mostly used in water purification processes, CO_2 reduction and NO_x decomposition. Additionally, according to its non-toxicity and and characteristic white color, it is also commonly used in food and cosmetics industry [8]. There is a disadvantage for TiO_2 photocatalysts that, widespread usage of them in water treatment applications are economically unavailable. This situation let the beginning of the search of an alternative photocatalyst.

ZnO, on the other hand, is reported to be an efficient photocatalyst and its lower cost makes ZnO the most appropiate candidate to replace TiO_2. Besides economic advantages, ZnO shows a better photocatalytic activity than TiO_2 in degradation of some organic pollutants in both acidic and basic media. Nanostructured ZnO has gained attention in the past two decades due to its wide band gap, stability, non-toxicity, photocatalytic activity and photosensitivity [14].

Surface area of zinc oxide nanoparticles are dependent on the synthesis method and it affects the photocatalytic activity of the photocatalyst, thus photocatalytic activity of zinc oxide is highly affected by the synthesis method. There is a disadvantage for ZnO photocatalyst that, its catalytic activity is still not high enough for the commercial applications [15].

2.5.1. Activation of a Semiconductor Photocatalyst in Visible Light

The parameters affecting the efficiency of a photocatalytic reaction can be listed as the type of pollutant to be degraded, type of the photocatalyst, concentration of both of the pollutant and the photocatalyst. Apart from these parameters, the wavelength and the intensity of the light irradiation is also important. TiO_2 and ZnO are UV photocatalysts and according to their wide band gap energy, their activity in visible light is low and the modification for making these photocatalysts sensitive to visible light is needed [16]. In order to increase the activity of these photocatalysts in visible light, several approches are offered. These approaches can be stated as the modification of these semiconductor photocatalysts with transition metals, semiconductor plasmon coupling, combining with non-metals and creating oxygen vacancies [17]. Quasi stable energy states are generated by these processes and the visible light photons are able to create excitons, leading the photocatalytic reaction.

Incorporation of crystalline defects in metal oxide semiconductors in the form of vacancies is an effective way to increase visible light absorption. The growth of single crystalline ZnO nanorods through hydrothermal processes and introducing oxygen vacancies to the nanocrystals have been reported extensively in the literature. Energy level and electron transition upon illumination with visible light for undoped and doped ZnO is given in figure 2.9 below.

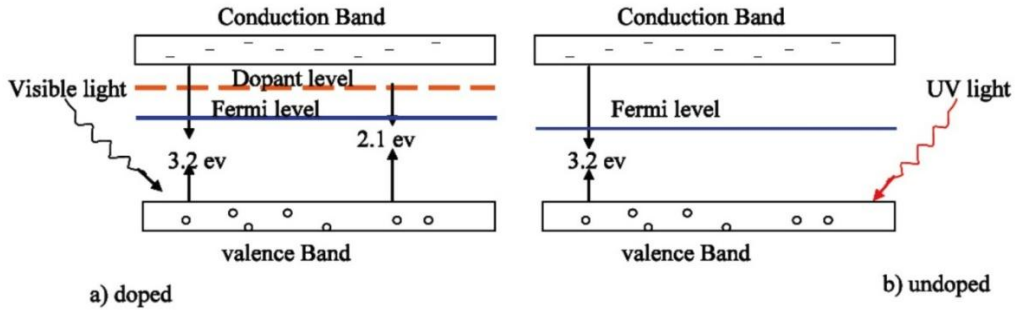

Figure 2.9. Representation of the energy level and electron transition upon illumination with visible light of doped (a) and undoped (b) ZnO [16]

2.6. Methods for Improving the Photocatalytic Activity of Semionductor Photocatalysts

It has been reported that the structural and morphologial properties of semiconductors affect the photocatalytic activity. These properties should be listed as the crystalline structure, shape, size, surface area and surface defects [18]. Synthesis methods are the dominant factors affecting the structural and morphological properties of semiconductor photocatalysts.

It should be noticed that the photocatalytic activity of a semiconductor is dependent on experimental conditions, properties of the catalyst and the properties of the organic species to

be degraded. If a catalyst shows a significant photcatalytic activity on one compound, this catalyst might not necessarily be the most appropiate catalyst for the degradation of other organic species [8].

Many researches are in the field of improving the photocatalytic activity of semiconductor photocatalysts, methods for improving the photocatalytic activity of semiconductor photocatalysts include doping, dye- sensitizing and semiconductor coupling and use of binary metal oxides [19].

2.6.1. Electron Donors

Electron donors are also known as sacrifical reagents or hole scavengers and they can react with the photo- generated valence band holes irreversibly. This reaction might increase the photocatalytic electron and hole separation ratio. Increase in this ratio also results an increase in th quantum efficiency. For a sustainable photocatalytic activity, electron donors should be added continously since they are consumed in the photocatalytic reaction [20].

Inorganic ions such as S^{2-}/SO_3^{2-} , Ce^{4+}/Ce^{3+} and IO_3^-/I^- are used as electron donors in photocatalysis. Hydrocarbons like EDTA, methanol, ethanol, lactic acid and formaldehyde are also widely used as electron donors and they are effective for improving the photocatalytic activity [5].

2.6.2. Doping

Doping is a process, where impurities are added in the structure of the semiconductor in order to improve its electrical properties. Band gap of the semiconductor can be altered by doping and excitation of the valence band electrons to the conduction band might be easier due to this induction.

Alkaline earth ions (Ca^{2+}, Sr^{2+}), rare earth ions (La^{3+}, Er^{3+}, Pr^{3+}) and noble metals (Pd^{2+}, Pt^{2+}, Au^{3+}, Ag^{+}) are used for doping processes [8].

The band gap of TiO_2 or ZnO decreases by doping with transition and noble metals. Decrease in the band gap means an increase in the light absorption capacity and shift in adsorption edge to visible light [5].

In this process, dopants act as traps for electrons and holes and they decrease the electron-hole recombination rate. Fermi energy levels of the dopants are lower than that of TiO_2 or ZnO. The excited electrons can be transferred to the metal particles, decreasing the electron- hole recombination rate. Fermi level shifts closer to the conduction band as electrons accumulate on metal particles acting as electron traps or active sites. Dopants also increase the interfacial charge transfer rate and thus increase the photocatalytic activity.

2.6.3. Dye- Sensitizing

Organic dyes such as erythrosin B, thionine and phthalo-cyanine are used for surface sensitization of TiO_2 photocatalysts [8]. The sensitivity of photocatalysts increase in the visible region and this increase can be explained as the injection of electrons from an excited level of the dye into the conduction band of semiconductor.

2.7. Applications of Semiconductor Photocatalysis

A good photocatalyst should have properties like availability, cost- effectiveness and chemical stability. TiO_2 and ZnO are the most widely used metal oxide semiconductor photocatalysts.

TiO_2 has been studied since 1980s and reported as the most efficient photocatalyst because it provides all these properties.

However, researches showed that ZnO can also be used as an effective photocatalyst like TiO_2 because their band gap energies are very close to each other, ZnO is cost effective also and it can even show a better performance than that of TiO_2 in degradation of organic molecules in both acidic and basic medium [45]. Some researches reported that ZnO shows a better photocatalytic efficiency than TiO_2 in aqueous medium [46]. ZnO has an advantage that its absorption capacity has a larger fraction of solar spectrum than that of TiO_2 [47]. However, in some studies, they have reported that the photocatalytic efficiency of ZnO decreases when it once is illuminated under UV- light. The decrease in the photocatalytic efficiency is based on the photocorrosion tendency [48]. The photocorrosion of ZnO can be prevented by keeping the catalyst in aqueous solutions in the dark [49].

2.7.1. Photocatalytic Degradation of Organic Pollutants

The development of novel heterogenous metal oxide semiconductor photocatalysts attracted considerable attention due to the photocatalytic effectiveness in the degradation of

environmental pollutants such as dyes, pesticides, detergents and volatile organic compounds under UV- light irradiation [45].

Heterogenous photocatalysis has attracted attention for water purification systems since it is more advantageous than conventional methods in terms of high capital investment, operation and maintenance cost.

Application of nanotechnology in water treatment systems includes the removal of the toxic hazardous substances and pollutants from water and production of smart materials or reactive surface coatings which are specifically engineered to the degradation or mineralization of a certain pollutant [16].

According to the mechanism of photocatalysis, photogenerated charge carriers occur. These photogenerated charge carriers and the molecules adsorbed on the surface of the photocatalyst undergo redox reaction. As a result of this redox reaction, the molecules adsorbed on the photocatalyst surface are being degraded. Photogenerated electrons and holes have high redox potentials and they are reported to be very efficient in degrading approximately all types of pollutants [50].

The basic process in photocatalysis is given as,

$$MO + h\nu \rightarrow MO(e^- + h^+) \quad (1)$$

where MO is the metal oxide semiconductor photocatalyst (i.e. TiO_2 or ZnO).

The formation of superoxide anions ($\cdot O_2^-$), hydrogenperoxide molecules (H_2O_2), hydroxyl radicals ($\cdot OH$), hydrogen dioxide anion (HO_2^-) and the hydroperoxy radicals ($\cdot HO_2$) are favored by the photogenerated electrons.

$$MO\ (e^-) + O_2 \rightarrow MO + \cdot O_2^- \quad (2)$$

$$MO\ (e^-) + \cdot O_2^- + 2H^+ \rightarrow MO + H_2O_2 \quad (3)$$

$$MO\ (e^-) + H_2O_2 \rightarrow MO + \cdot OH + OH^- \quad (4)$$

$$\cdot O_2^- + H_2O_2 \rightarrow \cdot OH + OH^- + O_2 \quad (5)$$

$$\cdot O_2^- + H^+ \rightarrow \cdot OH_2 \quad (6)$$

$$MO(e^-) + \cdot OH_2 \rightarrow MOHO_2^- \quad (7)$$

$$HO_2^- + H^+ \rightarrow H_2O_2 \quad (8)$$

$$2 \cdot OH_2 \rightarrow O_2 + H_2O_2 \quad (9)$$

Photogenerated holes also initiate oxidation reactions which are given below:

$$MO\ (h^+) + H_2O \rightarrow MO + \cdot OH + H^+ \quad (10)$$

$MO\ (h^+) + H_2O \rightarrow MO + \cdot OH + H^+$ (11)

$MO\ (h^+) + OH^- \rightarrow MO + \cdot OH$ (12)

The reactions are concluded as,

$\cdot OH + H^+ \rightarrow 2e^- + H_2O$ (13)

$\frac{1}{2}O_2 + 2H^+ \rightarrow +2eH_2O$ (14)

Surface area is an important parameter affecting the photocatalytic activity of the metal oxide semiconductor. Higher the surface area, higher the adsorption rate of the pollutant on the surface of the photocatalyst and higher the efficiency of the photocatalytic reaction.

Oxygen is also an important parameter in the photodecomposition of organic molecules on the catalyst surfaces since it results electron uptake. In order to predict this effect, kinetic models are developed. Number of the hydroxyl groups on the photocatalyst surfaces affect the adsorption rate of oxygen. It is also reported that, Langmuir- Hinshelwood is the best kinetic model describing the dependence of degradation rate constants of organic molecules on the dissolved oxygen concentration [51]. Zinc oxide has a large number of active sites on its surface and these active sites supply high surface reactivity and this photocatalyst is reported to be as efficient as TiO_2 in photocatalytic reactions.

Consequently, metal oxide nanoparticles are able to degrade both chemical and biological pollutants. There is a disadvantage for these nanoparticles that, they can not be easily removed after the treatment. The photocatalyst nanoparticles should be granulated into micron- size or they should be loaded onto highly porous substrates so the distribution of these nanoparticles into the environment can be prevented when they are used in flow- through water treatment plants. There is a serious concern that these nanoparticles might affect the environment, because the possible effects of these nanoparticles on human beings are not extensively understood yet. So, the photocatalyst nanoparticles should be regenerated and they should be conveniently removed. There is an important point that the nature of these nanoparticles, the behaviour and the interaction of these nanoparticles with the environment and human beings should be understood properly. If this point is considered, it might be possible to take precautions and design safer processes for the future [52].

Performance of a photocatalytic surface is determined by the measurement of the difference in the concentration of the organic pollutants deposited on the surface [53]. Methylene blue and stearic acid are the most widely employed probe molecules for this purpose.

2.7.2. Self- Cleaning Function

The wettability of solid surfaces is generally measured by water contact angle, which is defined as the angle between the solid surface and the tangent line of the liquid phase at the interface of the solid- liquid- gas phase [17]. When the photocatalyst surface is illuminated with UV

light, the contact angle of water decreases, means that it shows a tendency to spread out flat. When the contact angle reaches almost 0°, surface of the photocatalyst becomes completely non- water- repellant, defined as highly hydrophilic.

It is observed that there is a remarkable change in the wettability of the photocatalyst surface before and after UV light irradiation. Hydrophilicity of the photocatalysts lead the increase in the application fields.

When the photocatalyst surface is exposed to rain, the surface shows an effective self- cleaning function due to the hydrophilicity of the material. Stains on the surface are decomposed by photocatalytic reaction. TiO_2 coated materials are extensively used outdoors as photocatalytic building materials. Glasses, exterior tiles, PVC fabrics can be given as an example for the photocatalytic building materials. In figure 2.10, the difference between a conventional and TiO_2 coated tent material can be clearly seen when they are used outdoors.

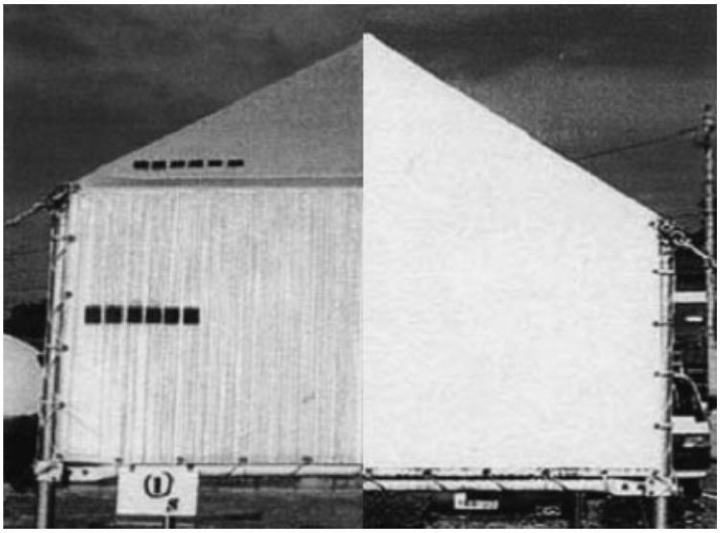

Figure 2.10. Conventional tent material (left) and TiO_2 coated tent material (right) [17]

2.7.3. Photocatalytic Antibacterial Effect

Photocatalytic reactions can be effective on the decomposition of biological agents. It is reported in the literature that, *E. Coli* microorganisms are completely disappeared when they are exposed to a UV light having an intensity of 1 mW/ cm^2 during one week. It is also reported that the time can be shortened to approximately 1 hour when the microorganisms are exposed to outdoor UV light. The shortening of the time is because outdoor UV light intensity is approximately three orders of magnitude stronger than indoor UV light intensity [54].

2.8. Vanadium Promoted Photocatalysts

According to their structural and electronic properties, vanadium oxides and vanadium oxide based catalysts have a special chemistry. First of all, d- orbitals of these compounds are partially filled and thus they have vast electronic, magnetic and catalytic properties.

Vanadium atoms present in five different oxidation states, varying from +2 to +5. These multiple oxidation states give vanadium an ability to be easily converted between oxides having different stoichiometries by oxidation and reduction.

Chemical and physical properties of vanadium oxide based catalysts are affected by the crystal faces which are taking place in the reaction, these crystal faces exist in two types in vanadium oxide based catalysts. First face is the one, where chemically saturated atoms expose metal cations with empty d-orbitals, behaving like electron acceptor sites, or oxygen ions bridging the metal- oxygen polyhedra. Second face is composed of unsaturated cations and anions. Excess charges are accumulated in unsaturated cations and anions and they generate significant variations on the potential along the catalyst surface. This crystalographic factor is connected with the electronic structure and it determines the chemical and catalytic properties of the catalyst [55].

Vanadium oxides transform from a semiconducting or insulating state to a metal phase at a critical temperature, resulting a change in the optical and electronic properties. Critical temperatures vary for each of the vanadium oxides, it is 68 °C for VO_2, whereas V_2O_5 undergoes this transition at 257 °C. Narrowness of the stability range of the stoichiometric vanadium oxides makes it difficult to prepare thin films of vanadium oxides. Oxides of vanadium, V_2O_3, V_3O_5, V_3O_7, V_4O_7,V_5O_9, V_6O_{11} and V_7O_{13} have a stability range near those of VO_2 and V_2O_5. [56].

The basic vanadium oxides are V_2O_5, VO_2, V_2O_3 and VO; the oxidation state of vanadium decreases from +5 to +2, respectively. Other forms of vanadium oxides are mixed valence oxides and they have a general formula of V_nO_{2n-1}, i.e. V_3O_5, V_4O_7, V_7O_{13}…etc.

V_2O_5 is an acidic oxide and it is orange-red in colour, slightly soluble in water and it forms a yellow- collodial solution when it is dissolved in water. V_2O_5 dissolves also in NaOH and it gives a colourless solution, containing vanadate ion (VO_4^{3-}). Vanadium ions are in the form of distorted octahedrons in the crystal structure [57]. V_2O_5 is thermodynamically the most stable vanadium oxide at normal temperature and pressure [61]. V_2O_5 undergoes a transition from a semiconductor to metal state at 257 °C.

VO_2 is dark blue in colour and it is obtained by the mild reduction of V_2O_5. VO_2 shows amphoteric characteristics. When it is dissolved in non- oxidizing acids, it gives the blue VO^{2+}, yellow to brown $V_4O_9^{2-}$ in alkali media and VO_4^{4-} at high pH. VO_2 has a rutile structure.

V_2O_3 is black in colour, shows basic characteristics and it is obtained by the reduction of V_2O_5 with hydrogen or carbon monoxide. It is soluble in aqueous acidic solutions and gives blue or green V^{3+}, this anion shows strong reducing properties. V_2O_3 has a corundum structure.

VO (or V_2O_2) is grey in colour, soluble in mineral acids and gives violet V^{2+}. VO shows metallic characteristics and it has a rock- salt structure [57].

Vanadium oxide based catalysts can be prepared via different methods. These metods will be described in detail in the following paragraphs.

Impregnation is the most simple and the most widely used method for the preparation of vanadium oxide based catalysts. Impregnation is the process, where aqueous or non- aqueous solution containing a vanadium oxide compound is adsorbed into the pores of an inorganic oxide.

Impregnation method can be applied in two different ways, first one is wet impregnation, where the support is dipped into an excess amount of solution. Second one is called as dry impregnation, pore volume impregnation or incipient wetness impregnation. Latter method can be applied in more controlled way, resulting the precise control of vanadium oxide loading.

Second step of impregnation method is contacting the support with a solution having a corresponding concentration or less of total pore volume of the support. This step enables the control of the active vanadium oxide concentration on the support. Loading rate can be affected by the solubility of the reagent and multiple impregnation steps may be necessary for the maximum obtainable loading. For example, V_2O_5 is slightly soluble in aqueous and non-aqueous solutions. Therefore, the preparation of the supported vanadium oxide catalysts is reported by two ways in many articles. Former way is impregnating the support with aqueous solution of NH_4VO_3, latter way is impregnating the support with a solution of NH_4VO_3 dissolved in oxalic acid.

Following step is the drying and heating process, allowing the connecting of vanadium oxide compounds onto the support oxide. Calcination is done in air at relatively high temperatures, i.e. 500 °C [57].

Grafting, being the second method for preparing vanadium oxide catalysts is defined as the dissipation of a vanadium containing compound from a solution. Dissipation occurs via the interaction with the hydroxyl groups on the surface of the inorganic support. Solutions used in order to obtain VO_x phases in grafting method are reported as $VOCl_3$ in CCl_4 or in benzene [58].

2.9. Effect of Vanadium on Zinc Oxide Thin Films

It is reported that doping might significantly affect the electrical and optical properties of wide band gap semiconductor materials. Theoritical studies showed that vanadium might lead room temperature ferromagnetism (RTFM) when it is doped with semiconducting oxides [59]. Articles investigating the effect of vanadium on zinc oxide have generally dealt with the change in the optical, electrical, magnetic, ferromagnetic properties, structural defects and conductivity. The effects of annealing on the magnetic properties have also been investigated [60]. Vanadium concentration is also an important parameter on the structural and magnetic properties of thin films. Articles investigating the effect of vanadium concentration report that doping concentration and crystalline microstructure signifcantly affects the magnetic characteristics. Films with the lowest doping concentrations (2%) exhibited weak ferromagnetism and increase in the vanadium concentration resulted a degradation of the magnetic ordering [61]. Vanadium concentration is also effective in saturation magnetization, increase in concentration increases the saturation magnetization.

It is reported that the defect states and covalent bonds in ZnO are sensitive to dilute amount of vanadium. Vanadium loading may result the changes in the band gap [62].

CHAPTER 3

EXPERIMENTAL

In this study, ZnO and vanadium doped ZnO thin films over ITO coated glass substrates were obtained by electrodeposition technique. Obtained thin film samples were characterized by using XRD, UV-Vis and the photocatalytic activity of the samples were determined for methylene blue and stearic acid degradation.

3.1. Pre-Treatment of ITO Glass Sheets and Preparation of the Electrode

ITO glass substrates, having a dimension of 2x5 cm, were cleaned with acetone (Merck, CAS No: 67-64-1) and isopropanol (Sigma- Aldrich, CAS No: 67-63-0), respectively. The substrates were then rinsed with pure water and dried at room temperature for 30 minutes.

Platinum (Pt) wires were attached into pre cleaned ITO substrates bu using conductive silver glue (Spi Supplies, CAS No: 7440-22-4) which is cured in oven at 80 °C for 2 hours.

3.2. Preparation of Electrodeposition Solution

Electrodeposition of ZnO was achieved by using $ZnCl_2$ (Merck, CAS No: 7646-85-7) solution as electrolyte. KCl (Merck, CAS No: 7447-40-7) to enhance electrical conductivity, benzoic acid (C_6H_5COOH, (Merck, CAS No: 65-85-0) as catalyst and sodiumlaurylsulfate ($NaC_{12}H_{25}SO_4$, Sigma- Aldrich, CAS No: 151-21-3) as surfactant. The concentrations of these additives in electrodeposition solution were 2 M, 0.2 M, 0.2 M and 0.2 M, respectively.

Benzoic acid was used as the small negatively charged additive. It increases the current density with the number of functional groups during electrodeposition.

Sodiumlaurylsulfate was used as surfactant. It is known that sodiumlaurylsulfate affects the growth rate of ZnO layer, but is is also reported that sodiumlaurylsulfate do not have any effect on the morphology of the resulting ZnO thin films [35]

3.3. Preparation of ZnO Thin Films by Electrodeposition

Electrodeposition process was performed by using Perkin- Elmer electroanalyzer. (figure 3.1) and DC supply for the samples prepared at room temperature and at 70 °C, respectively. Pre-treated ITO glass sheets and pure Zn wire were used as anode and cathode, respectively. Saturated calomel electrode was employed as the reference electrode.

Electrodeposition was performed at 25 °C and 4.0 VDC potential was applied to the solution during 20 hours for the samples prepared at room temperature and 1.2 VDC potential was applied during 30 minutes for the samples prepared at 70 °C.

After electrodeposition, coated samples were cleaned with ethanol (Sigma- Aldrich, CAS No: 64-17-5), rinsed with water and finally dried in oven in 80 °C for 30 minutes. Ethanol is used in order to rinse the sample from SDS.

The final step is the calcination of the samples, at 500 °C in air for 15 minutes.

Figure 3.1. Controlled potential electroanalyzer

3.4. Synthesis of Vanadium Doped Samples

Methylene blue photodecomposition studies showed that the films were photocatalytically active. This part of the experimental procedure is about the improvement of the photocatalytic activity of the prepared ZnO thin films and investigate the effect of vanadium doping on the optical properties of ZnO thin films.

Vanadium doping was performed by both an aqueous solution of ammonium metavanadate (Merck, CAS No: 7803-55-6) and ammonium metavanadate dissolved in oxalic acid (Horasan Kimya, Purity: 99.5%). The concentrations of these solutions are 0.4 g NH_4VO_3 / 100 ml H_2O and equimolar solution of $(COOH)_2$ and NH_4VO_3, respectively.

It is stated in the literature that vanadium is in (+5) oxidation state in aqueous ammonium metavanadate solution. Oxalic acid acts as a reducing agent and vanadium is in (+4) oxidation state in the latter solution [57].

The color of the prepared solutions also gives information about the oxidation state of vanadium. It is reported that the most important oxidation states in aqueous solutons are V^{5+} and V^{4+}, the formation of the other specific vanadium oxides is dependent on the pH of the solution and concentration of vanadium oxide. V_2O_5, in which the oxidation state of vanadium is (+5), is slightly soluble in water and it gives a pale yellow solution with collodial character (figure 3.2, left). When NH_4VO_3 is dissolved in aqueous oxalic acid it forms a dark coloured solution (figure 3.2, right) and the oxidation of vanadium reduces to (+4) because oxalic acid acts as a reducing agent [57].

Figure 3.2. Ammonium metavanadate solutions dissolved in water (left) and oxalic acid (right)

When the aqueous NH_4VO_3 and NH_4VO_3 + $(COOH)_2$ solutions were prepared, ZnO coated ITO glass sheets were coated with these solutions by dip coating method individually.

Dip coating was performed via dip coating apparatus (figure 3.3.). The samples were immersed to the solution with a speed of 20 mm/ sec, waited for 1 minute in the solution and pulled back with a speed of 2 mm/sec.

Figure 3.3. Dip coating apparatus

After dip coating process, the samples were dried at ambient conditions (room temperature). Since VO_2 undergoes a transition from a semiconductor to metal phase near 68 °C, drying of these samples at higher temperatures was avoided [56].

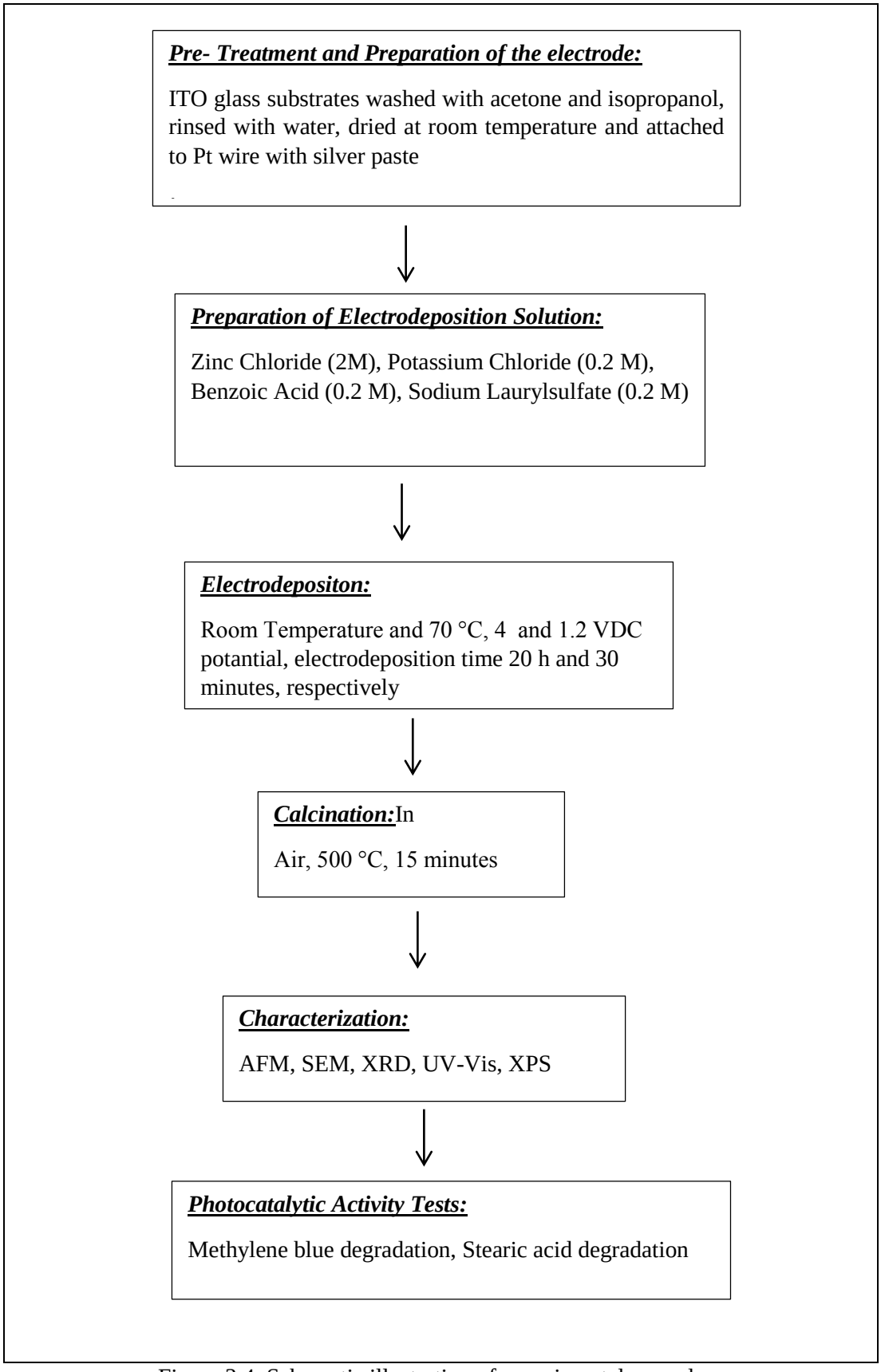

Figure 3.4. Schematic illustration of experimental procedure

3.5. Characterization

3.5.1. Band Gap Calculations

Band gap calculations of ZnO coated and V/ZnO samples were calculated using the absorbance data in the UV- Vis region. This absorbance data was obtained between 200- 800 nm using Schimadzu 2550 UV- Vis spectrophotometer by using ITO glass as reference.

UV- Vis spectroscopy can be used in te measurement of band gap or optical absorption edge energy depending on the spectra. Photon energy corresponding to the band gap occurs at the onset of intense optical absorption, providing an experimental method for the determination of the band gap [1].

For a direct band gap, *a,* absorption coefficient, is related with the formula given below:

$a = A^* \sqrt{hv - Eg}$

Here,

hv is energy, which can also be written as (h*c)/λ, where,

h: Planck's constant (6.626×10^{-34} kgm^2/s)

c: Speed of light (3×10^8 m/s)

λ: Wavelength (m)

A* is a frequency- independent constant

E_g is the band gap energy

For an indirect band gap, the formula changes as,

$$a = \frac{(hv - E_g + E_p)2}{\exp\left(\frac{E_p}{kT}\right) - 1} + \frac{(hv - E_g - E_p)2}{1 - \exp(-\frac{Ep}{kT})}$$

Here,

E_p is phonon energy,

k is the Boltzmann constant ($8.6173324(78) \times 10^{-5}$ eVK^{-1})

T is the thermodynamic temperature

Intercept of $(a*hv)^n$ vs hv yields the band gap energy. If the (a*hv)^2 vs hv plot forms a straight line, it can be inferred that there is a direct band gap and the direct band gap value can be calculated as extrapolating the straight line to the energy axis. If the (a*hv)^(1/2) vs hv plot gives a straight line, it can be inferred that there is an indirect band gap and the indirect band gap value can be calculated as extrapolating the straight linet o the energy axis, assuming that the phonon energy is equal to zero.

3.5.2. Surface Imaging with Atomic Force Microscopy (AFM)

Surface images of the thin film samples were obtained by Nanosurf Easyscan 2 (figure 3.5). The AFM images were used to characterize the surface roughness of thin film samples. AFM was operated in non contact dynamic force mode. The probe used for surface imaging was silicon SPM- sensor with a thickness of 7 μm, length of 225 μm and a width of 38 μm and the detector side of the sensor was Al- coated. The obtained images were utilized for the analysis of the surface rouhgness of the thin films.

Figure 3.5. Nanosurf easyscan 2

3.5.3. Surface Imaging with Scanning Electron Microscopy (SEM)

Surface images of the thin film samples were obtained by Quanta 400 F Field Emission Scanning Electron Microscopy in METU Central Laboratory. Obtained SEM images were utilized in order to characterize the morphology of the thin film samples. The samples were not pre- treated with Au-Pd before SEM analysis because they were conductive enough.

3.5.4. X-Ray Diffraction (XRD)

X-Ray diffraction (XRD) data of the samples were obtained by Rigaku Ultima- IV diffractometer in METU Central Laboratory. Scan range of the X- Ray diffractograms were between angles (2θ) of 20° to 80° with a grazing angle of 0.5° and scanning speed of 1.000 deg/min. Diffractograms were taken by using Cu source (λ=1.5405 Å).

The crystal structure of the thin films were characterized by the obtained X-Ray diffraction patterns and they were compared with Joint Committee on Powder Diffraction Standards (JCPDS) files.

3.5.5. X-Ray Photoelectron Spectroscopy (XPS)

X-Ray photoelectron spectroscopy (XPS) data of the thin film samples were obtained by PHI 5000 VersaProbe in METU Central Laboratory. XPS data were utilized in order to characterize the surface composition and determine the electronic states of the elements in the thin film samples.

Electronic states of V, Zn and O were determined between 536- 511 eV for V2p, 543- 523 eV for O1s, 1036- 1016 eV for Zn2p3 and 1055- 1035 eV for Zn2p1 and the obtained spectra were corrected according to the carbon peak at 285 eV.

3.6. Photocatalytic Activity Tests

3.6.1. Methylene Blue Degradation Tests

Methylene blue degradation reactions gave information about the photocatalytic activity of ZnO and V-ZnO thin film samples on ITO glasses.

Some pre-tests were performed to determine the optimum MB concentration for degradation tests. 3, 20, 50 and 100 ppm MB (Merck, CAS No: 61-73-4) solutions were prepared and thin film samples electrodeposited in room temperature during 20 hours were immersed to these solutions for 24 hours and MB absorption spectra were obtained and degradation tests were performed. Optimum results were obtained with 20 ppm MB solution. Photocatalytic activity tests with MB degradation reaction procedure is as follows:

Firstly, UV- Vis spectra of the samples prepared at room temperature during 20 hours were obtained before they were immersed to methylene blue solution. UV- Vis absorbance data were obtained between 200- 800 nm using Schimadzu 2550 UV- Vis spectrophotometer in spectrum mode. Uncoated and untreated ITO glass sheet was employed as reference cell.

Thin film samples were then immersed to 20 ppm MB solution and they were kept in dark during 24 hours, then UV- Vis spectra of the samples were obtained again, being careful for obtaining the data from the same spot. The difference between two spectra obtained before and after immersing to MB solution was used to determine whether MB is adsorbed on thin

film samples. The expected difference between these two spectra is the observing the MB peak between 600- 650 nm.

Degradation reaction was started by exposing the thin film samples to the artificial solar irradiation with a power of 300 W/m^2 between 280- 780 nm by using SUNTEST CPS+ solar simulator shown in Figure 3.6.

Time course of degradation reaction was followed by removing the samples at every 20 min of exposure and measuring the absorbance value at 665 nm which corressponds to the methylene blue concentration. During absorbance measurements, uncoated ITO substrates were used as reference.

Figure 3.6. SUNTEST CPS+ solar simulator

MB degradation tests were also applied on ZnO and V-ZnO thin film samples by exposing them to 15 W, 254 nm UV irradiaton for 5 minute intervals and recording the MB absorbance data at 665 nm.

3.6.2. Stearic Acid Degradation Tests

Stearic acid degradation tests also gives information about the photocatalytic activity of the ZnO and V-ZnO thin films.

Stearic acid solution was prepared by dissolving stearic acid (Surechem Products, Product No: S7682) in carbon tetrachloride (Carlo Erba Reagents, CAS No: 56-23-5). Stearic acid was coated on thin film samples by dip coating method and the solution concentration was 40 g $CH_3(CH)_{16}COOH$ / 75 ml CCl_4.

Photocatalytic decomposition of stearic acid coated on ZnO and V-ZnO thin films were monitored by Bruker Equinox 55 FT-IR spectroscopy. FT-IR spectra of stearic acid coated thin film samples were first obtained (background: air) before they are exposed to UV light.

Degradation reaction was started by exposing the thin film samples to 36 W, 254 nm UV-C lamp for 90 minutes and FT-IR spectra were obtained from the same spot and the difference in the asymmetric C-H streching modes of CH_3 groups and the symmetric- asymmetric C-H streching modes of CH_2 groups in the region 2700-3000 cm^{-1} was monitored. This procedure was repeated for 90 minute intervals until the degradation rate of stearic acid stabilizes.

CHAPTER 4

RESULTS AND DISCUSSION

The main objective of this study was the preparation of photocatalytically active ZnO thin films deposited on ITO glass sheets by electrodeposition method. ZnO and vanadium doped (V/ZnO) thin film samples were prepared by electrodeposition at both room temperature and 70 °C.

The effect of electrodeposition time, synthesis temperature, concentration of electrodeposition solution and vanadium doping on the photocatalytic activity of thin film samples were examined.

4.1. Characterization

Structural and morphological properties of thin film samples were characterized by UV-Vis spectroscopy, AFM, SEM, XRD and XPS.

Band gap of the samples was determined by using UV-Vis spectroscopy. AFM images gave information about the surface roughness of the samples, Surface morphology was examined by using SEM images. The chemical composition of the thin films were determined by using EDAX analysis. X-Ray diffraction analysis was performed to determine the crystal structure of ZnO. The surface composition and oxidation state of zinc and vanadium were determined by using X-Ray photoelectron spectroscopy (XPS) data.

4.1.1. Band Gap Calculations

Band gap of the material is the difference between the energy level of valence band and conduction band electrons. When conduction band electron is transferred to valence band, photon is emitted if the momentum of electron and holes are the same. In this case, the energy of photons corresponds to direct band gap. If the momentum of electron and valence band holes are different, electrons pass through an intermediate state, and photon cannot be emitted.

In this case, the difference between the energy level of conduction band and valence band electrons is called indirect band gap. UV- Vis spectroscopy can be used for the measurement of band gap or optical absorption edge energy.

Band gap calculations of ZnO and V-ZnO thin film samples were performed using the absorbance data obtained between 200-800 nm in UV-Vis region by using uncoated ITO samples as reference.

For semiconductors, the absorption coeffcient is proportional with the frequency of light and band gap energy of material. Therefore, intercept of $(a*hv)^n$ vs hv yields the band gap energy. Here,

α is absorbance,

hv is energy, which can also be written as (h*c)/λ, where,

h: Planck's constant ($6.626x10^{-34}$ kgm^2/s)

c: Speed of light ($3x10^8$ m/s)

λ: Wavelength (m)

The value n is choosen as 2 and ½ for direct and indirect band gap, respectively.

As mentioned in the experimental procedure, thin film samples were prepared at both room temperature and at 70 °C.

First experiments were performed in order to determine the effect of electrodeposition time on the band gap of the samples. Five different samples were prepared by applying 4 volts DC during 9, 16, 20, 30 and 40 hours at room temperature.

After electrodeposition, absorbance data of the ZnO thin film samples were obtained between 200-800 nm in UV-Vis region. (α**hv*)^2 vs (*hv*) and (α* *hv*)^(1/2) vs (*hv*) plots were plotted and the calculated direct and indirect band gap values were compared with the literature value which is measured for bulk ZnO samples.

Absorbance data of thin film samples prepared at room temperature have very small values when compared to the absorbance data of thin film samples prepared at 70 °C. This might be due to lower electrodeposition rate at lower temperatures, resulting a lower film thickness.

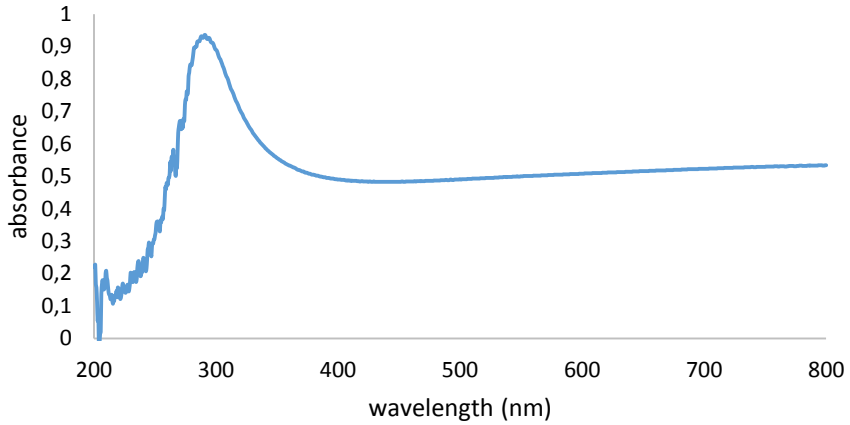

Figure 4.1. UV-Vis spectrum of ZnO thin film over ITO glass sample prepared at room temperature, 4 VDC for 20 hours

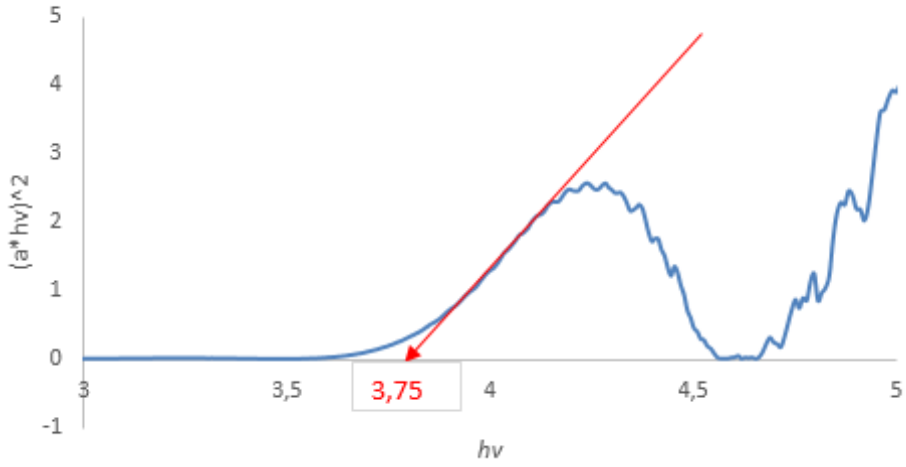

Figure 4.2. (a*hv)^2 vs *hv* plot of ZnO thin film over ITO glass sample prepared at room temperature, 4 VDC for 20 hours

Extrapolating the linear parts to x- axis (photon energy axis) gives the direct band gap value of the sample. Band gap of the ZnO thin film electrodeposited for 20 hours at room temperature was measured as 3.75 eV.

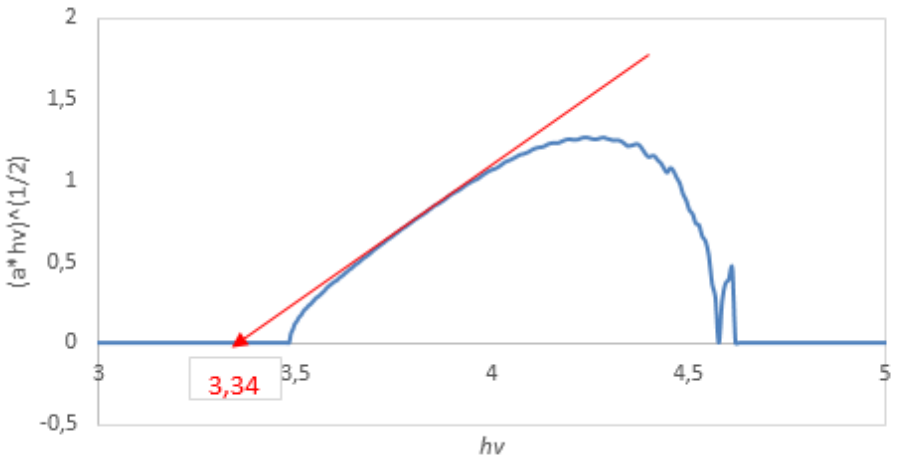

Figure 4.3. (a*hv)^(1/2) vs *hv* plot of ZnO over ITO glass sample prepared at room temperature, 4 VDC, 20 hours

Similarly, extrapolating the linear region to x- axis (photon energy axis) yields the indirect band gap value of the sample. Band gap of the ZnO thin film electrodeposited for 20 hours at room temperature, 4 VDC was measured as 3.34 eV, which is in good aggreement with the literature value (3.36 eV) [66]

The effect of electrodeposition temperature was examined by measuring the band gap values of samples prepared at 70 °C. The rate of electrodeposition is affected by the electrodeposition temperature.

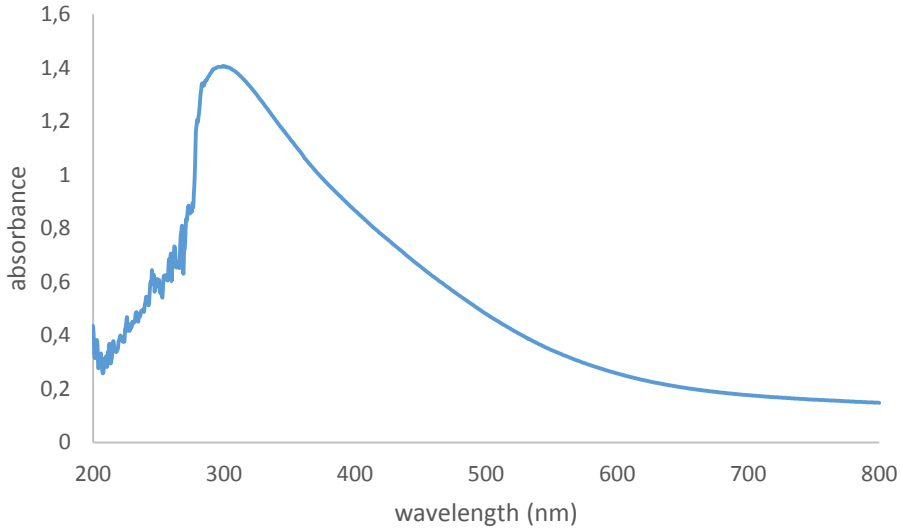

Figure 4.4. UV-Vis spectrum of ZnO thin film sample prepared at 70 °C, 1.2 VDC for 30 minutes,

Direct and indirect band gap plots of the sample prepared at 70 °C are depicted in figures 4.5 and 4.6, respectively.

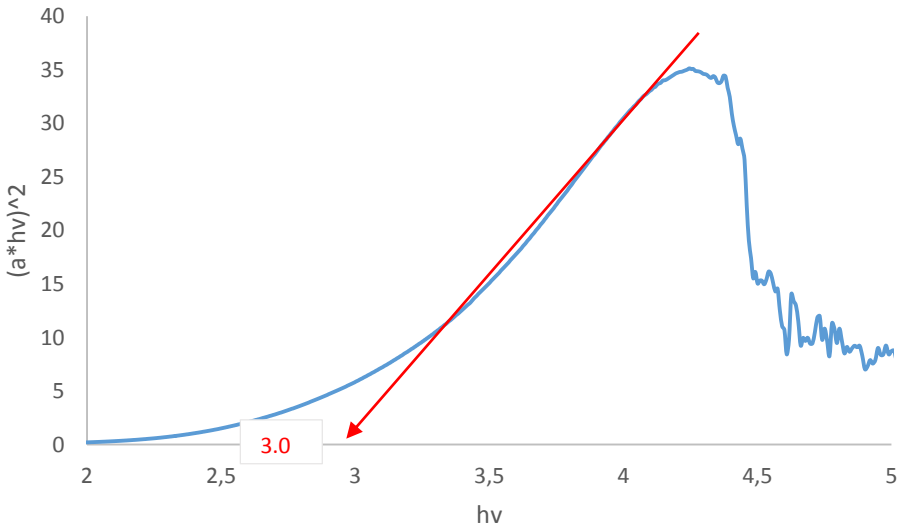

Figure 4.5. (a*hv)^2 vs *hv* plot for the ZnO thin film over ITO glass sample prepared at 70 °C, 1.2 VDC for 30 minutes

(a*hv)^2 vs hv plot of ZnO thin film prepared at 70 °C during 30 minutes is given in Figure 4.5. Extrapolating the linear parts to x- axis gives the direct band gap value of the sample, which was measured as 3.0 eV.

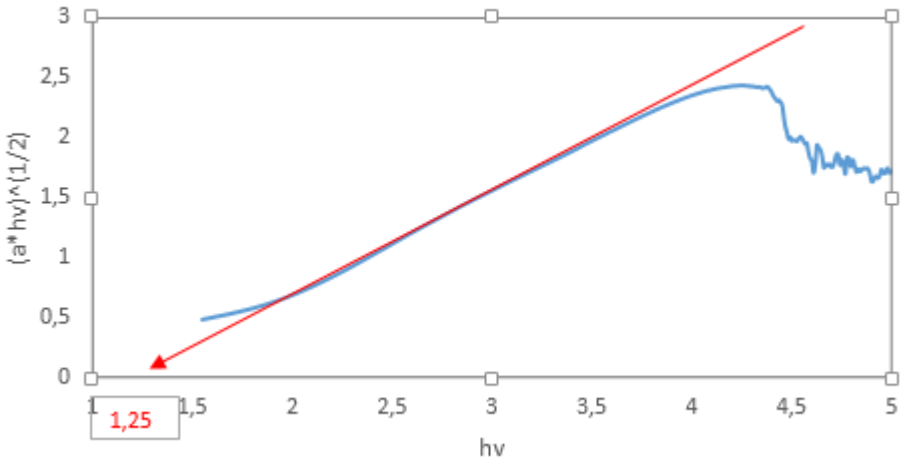

Figure 4.6. (a*hv)^(1/2) vs *hv* plot for the ZnO thin film over ITO glass sample prepared at 70 °C, 1.2 VDC for 30 minutes

Figure 4.6 shows the (a*hv)^(1/2) vs hv plot of ZnO thin film prepared at 70 °C during 30 minutes. Extrapolating the linear parts to x- axis gives the indirect band gap value for this sample, which was measured as 1.25 eV.

Measured direct and indirect band gap energy values for the samples prepared at room temperature during 20 hours and at 70 °C during 30 minutes are given in Table 4.1 for better comparison.

Table 4.1. Measured direct and indirect band gap energy values for the samples prepared at room temperature and 70 °C

Sample	Direct Band Gap (eV)	Indirect Band Gap (eV)
Room Temperature, 4 VDC, 20 h	3.75	3.34
70 ° C, 1.2 VDC, 30 min	3.0	1.25

Zinc oxide is a semiconductor material exhibiting 3.36 eV band gap. The sample prepared at room temperature, yield 3.34 eV direct band gap, and the sample prepared at 70 °C, lower band gap was determined (3.0 eV). Higher temperature allows the formation of thin films having higher crystallinity with less defects. The oxidation rate of Zn^{+2} ions is low at room temperature which allows the formation of thin film with more amorphous structure. As it can be seen from figures 4.1 and 4.4, larger film thickness of ZnO layer at 70^{o}C than the one at 20^{o}C is evidenced by higher absorption of UV light. The difference between the measured direct and indirect band gap energy values might be explained by structural properties such as crystal defects, impurities, particle size, surface area etc. Therefore, it might be suggested as the thin film sample prepared at 70^{o}C will perform better photocatalytic activity than the sample prepared at 20^{o}C under solar irradiation harvesting more photons from visible light.

The photocatalytic activity of zinc oxide significantly depends on the optical and electronic properties and the photocatalytic activity can be improved by doping with transition metals. Doping may cause significant change in band structure of semiconductor, which can be observed by the change in optical properties. Therefore, the effect of vanadium doping on the optical properties of zinc oxide thin films were also examined by UV- Vis spectroscopy. ZnO thin films were impregnated by aqueous solution of NH_4VO_3 by using dip coating technique. These samples were named as V^{+5} doped samples.

UV-Vis absorbance data of vanadium doped zinc oxide thin film samples prepared at room temperature and 70 °C were compared with undoped ZnO thin film samples. Figure 4.7 shows the UV-Vis spectrum of the sample prepared at room temperature before and after vanadium doping.

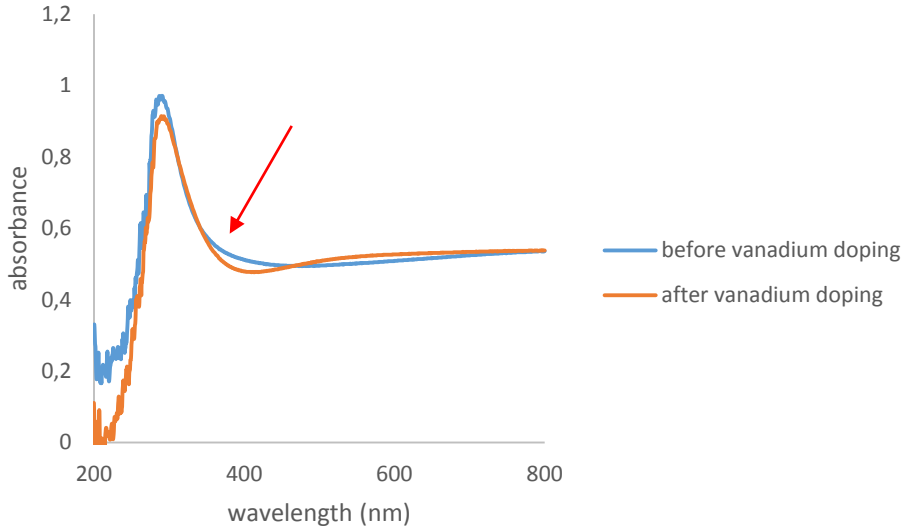

Figure 4.7. UV-Vis spectra of V^{+5} doped and undoped ZnO thin film samples prepared at room temperature, 4 VDC for 20 hours

The decrease in the absorbance data after V^{+5} doping near 400 nm can be clearly seen in figure 4.7. The red shift in absorption edge or shift in the band gap energy to visible light indicates the success of vanadium doping.

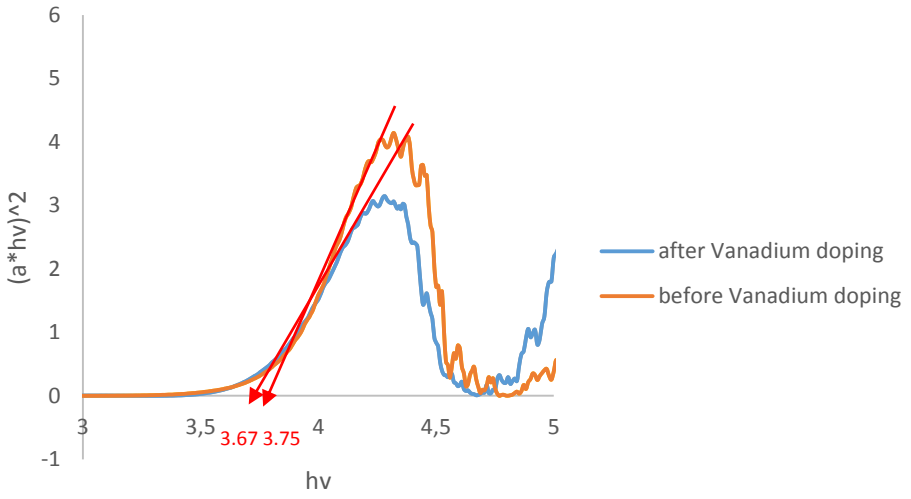

Figure 4.8. Effect of V^{+5} doping on the band gap enery of the sample prepared at room temperature, 4VDC for 20 hours

Figure 4.8 summarizes the effect of V^{+5} doping on direct band gap energy for the sample prepared at room temperature. Band gap energy of this sample was measured as 3.75 and 3.67

eV before and after V^{+5} doping, respectively. Similar results were also obtained for the samples prepared at 70 °C (figures 4.9 and 4.10). However the effect of V^{+5} doping is more apperant at 70°C than 20°C. The higher crystallinity of ZnO film prepared at 70°C appears to be more effected by the presence of vanadium impurities. Figures 4.9 and 4.10 shows the UV-Vis spectra of the sample prepared at 70 °C and the change in the band gap energy before and after V^{+5} doping, respectively.

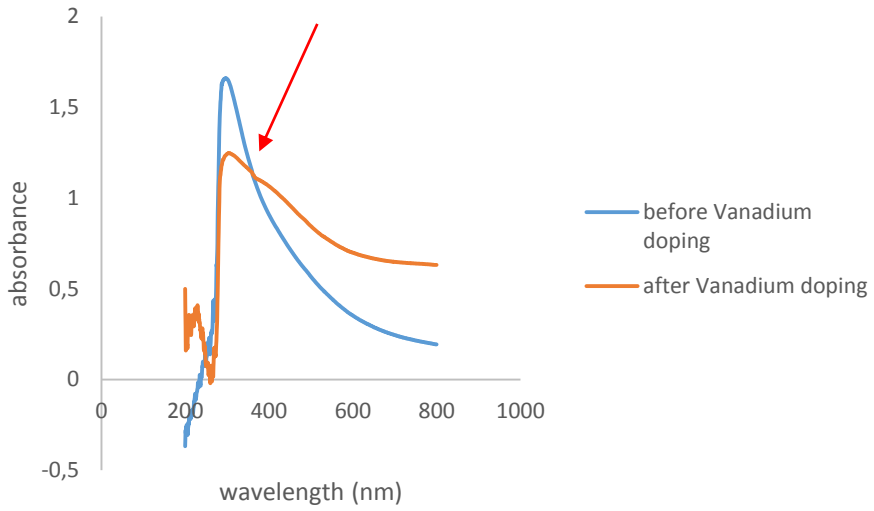

Figure 4.9. UV-Vis spectra of V^{+5} doped and undoped ZnO thin film samples prepared at 70°C, 1.2 VDC for 30 minutes

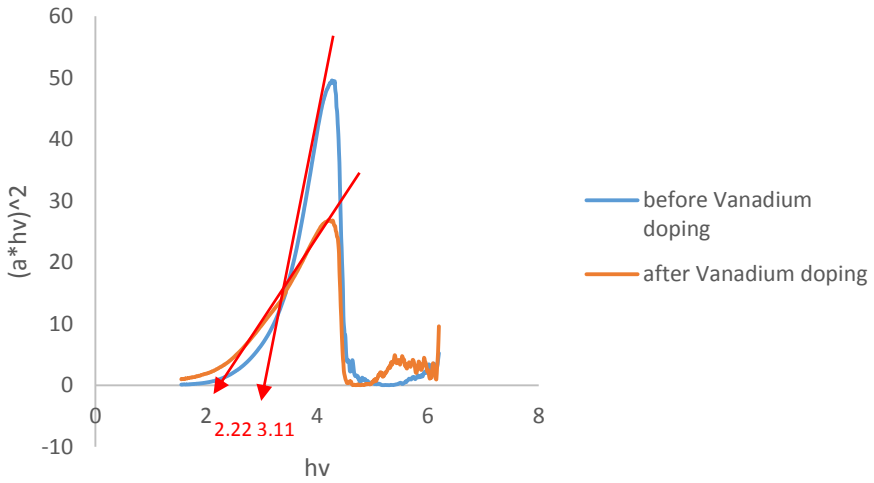

Figure 4.10. Figure 4.10. Effect of V^{+5} doping on the direct band gap enery of the sample prepared at 70 °C, 1.2 VDC for 30 minutes

Band gap of the samples prepared at 70 °C was measured as 3.11 and 2.22 eV before and after vanadium doping, respectively.

Table 4.2. Measured direct band gap energy values for the samples prepared at room temperature and 70 °C before and after V^{+5} doping

Sample	Before V^{+5}doping	After V^{+5} doping
Room Temperature, 20h	3.75	3.67
70 ° C, 20 min	3.11	2.22

Band gap of the V^{+5} doped and undoped ZnO thin film samples are summarized in Table 4.2. The band gap energy of the sample prepared at room temperature was measured as 3.75 and 3.67 eV before and after V^{+5} doping, respectively. For the sample prepared at 70 °C, the measured band gap values were 3.11 and 2.22 eV before and after V^{+5} doping. Band gap of the ZnO thin film samples prepared at 70°C temperature have much lower band gap values than those of which were prepared at 20 °C and the presence of vanadium cause higher shift on the band gap and of ZnO prepared at 70°C. These results indicate that the photocatalytic activity of the thin film samples can be improved by vanadium doping.

In order to observe the effect of vanadium oxidation states on the band gap energy of ZnO thin films, oxalic acid reduction method was also used. For this purpose, oxalic acid was added into NH_4VO_3 solution and another set of ZnO thin film samples were impregnated by dip coating method. These samples were coded as V^{+4} doped samples. The effect of V^{+4} doping on ZnO thin films samples is shown in Figure 4.11.

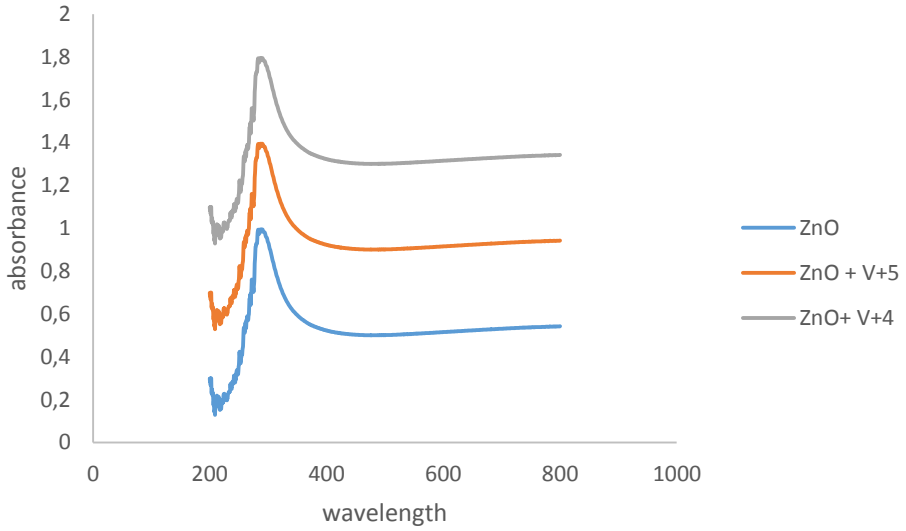

Figure 4.11. UV-Vis absorption spectra of V^{+5}-and V^{+4} doped and undoped ZnO thin films prepared at70 °C and room temperature, 1.2 VDC and 4 VDC for 30 minutes and 20 hours, respectively

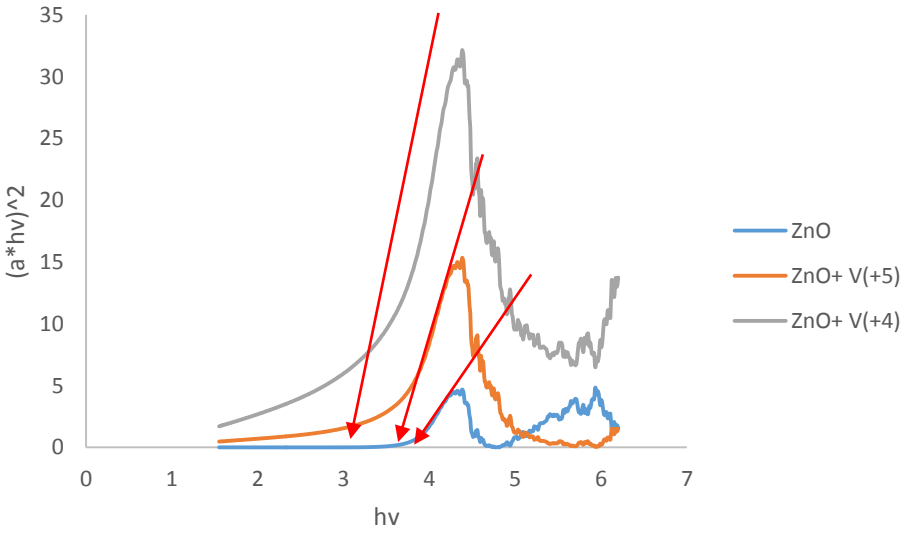

Figure 4.12. Direct band gap of of V^{+5}-and V^{+4} doped and undoped ZnO thin films prepared at70 °C and room temperature, 1.2 VDC and 4 VDC for 30 minutes and 20 hours, respectively

Measured direct band gap of the samples were 3.75 eV, 3.71 eV and 3.35 eV for ZnO thin film, V^{+5} doped and V^{+4} doped ZnO thin film, respectively. It is clear that, +4 state of vanadium has more impact on the band gap than +5 state. Vanadium doped zinc oxide thin films have significantly lower direct band gaps. Sample prepared by aqueous solution of ammonium

metavanadate (V^{+5}) has a direct band gap of 3.71 eV, whereas sample prepared by ammonuium metavanadate dissolved in oxalic acid solution (V^{+4}) has a direct band gap of 3.35 eV in room temperature. As the oxidation state of vanadium decreases, band gap value of the sample also decreases.

It can be said that, the photocatalytic activity of the samples prepared at 70 °C might be higher than the samples prepared at room temperature. This result can be explained as the higher deposition rate of ZnO at 70 °C. However, the result nearest band gap value to the literature was observed at the sample prepared at room temperature as 3.34 eV.

Doping zinc oxide thin film samples with vanadium ions improved their optical properties, resulting a decrease in their band gap energy values. The oxidation state of vanadium is also found as important parameter to harvest more photons from visible light spectrum.

As a result, doping zinc oxide thin film samples with vanadium had improved their optical properties, resulting a decrease in their band gap energy values. Doping ZnO with vanadium ions is an effective and promising way to modifiy the band gap and photocatalytic activity.

4.1.2. Surface Imaging with SEM

SEM images of the samples of both electrodeposited ZnO thin film at room temperature and at 70 °C were examined. In addition, V^{+4} and V^{+5} doped ZnO samples were also analyzed to observe any change in textural properties. The effect of temperature on the growth and morphology can be clearly observed from the SEM images of the samples. Additionally, EDAX analysis were also obtained in order to correct the composition of the thin films.

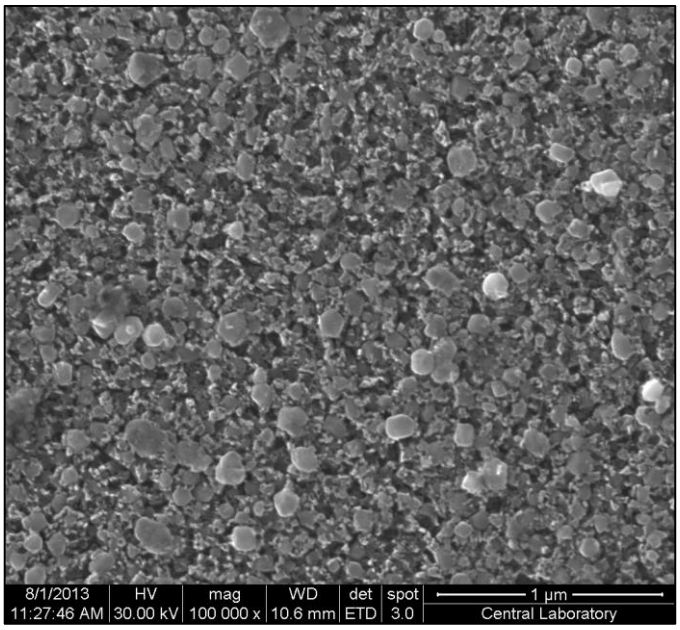

Figure 4.13. SEM image of ZnO thin film electrodeposited at room temperature, 4 VDC for 20 hours

Figure 4.13 shows the SEM image of the sample electrodeposited at room temperature. The surface of the film is comprised of uniform ZnO nanoparticles. EDAX analysis of this sample showed that the weight percentage of Zn of this sample was 2.11%. (Appendix A)

Increase in the synthesis temperature was observed to have a significant effect on the morphology of the ZnO thin film. Figures 4.14 and 4.15 show the SEM images obtained from different spots of the same sample, ZnO thin film sample electrodeposied at 70 °C.

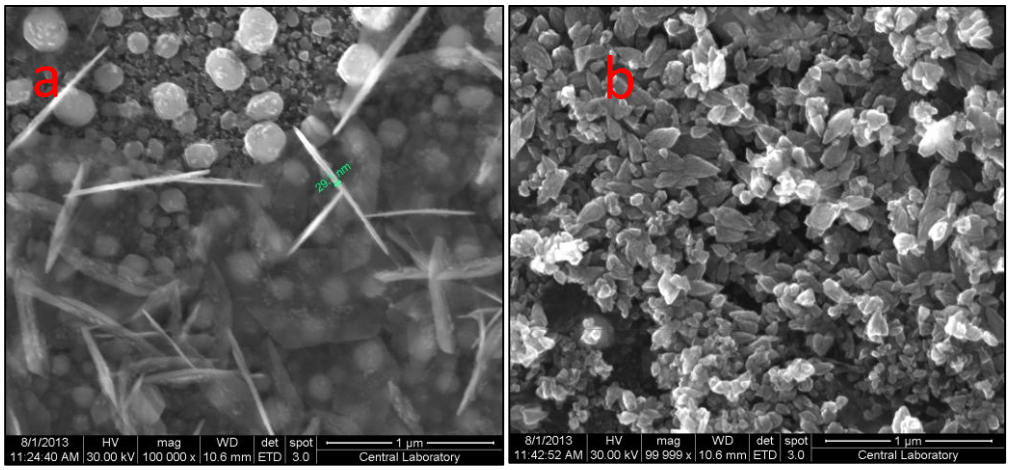

Figure 4.14. SEM images of ZnO thin film electrodeposited at 70 °C, a) formation of nanoplates, b) deposition of nanoplates

Increase in the temperature affected the morphology of the sample, ZnO nanoparticles tended to form nanoplates with an approximate diameter of 30 nm. However, due to the non-homogenity, the composition of Zn of the sample might change at different spots of the sample. The samples prepared at 70°C shows the formation of bulk ZnO films which the EDAX analysis yield 80% Zn.

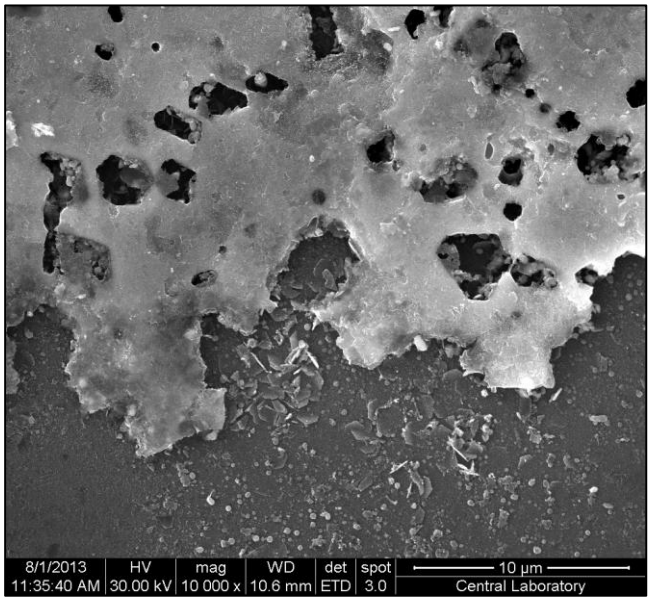

Figure 4.15. SEM image of ZnO thin film electrodeposited at 70 °C

SEM images of both of the samples might give information about the growth mechanism of ZnO. At room temperature, ZnO was spherical in shape and the surface was homogenous.

Increase in the temperature resulted the formation of nanoplates which are transformed into continous ZnO film. Also the calcination step has an important role on the sintering and film formation.

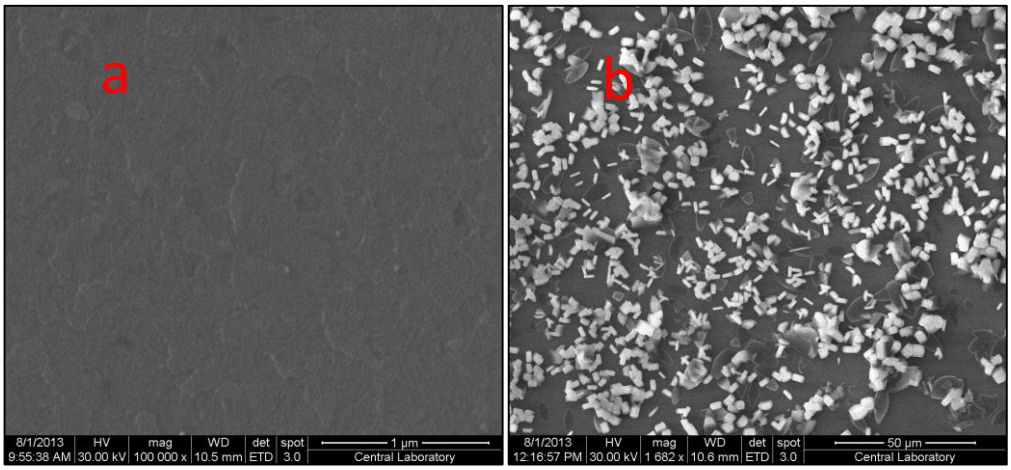

Figure 4.16. SEM image of the sample electrodeposited at room temperature, a) ZnO, b) V^{+5} , 4 VDC for 20 hours

Figure 4.16 shows the SEM image of the sample electrodeposited at room temperature and dip coated with the aqueous solution of NH_4VO_3. Vanadium was not deposited on the surface homogenously, and the EDAX analysis obtained for this sample showed that the weight percentage of ZnO and V of this sample was 4.19 and 2.40%, respectively. (Appendix A)

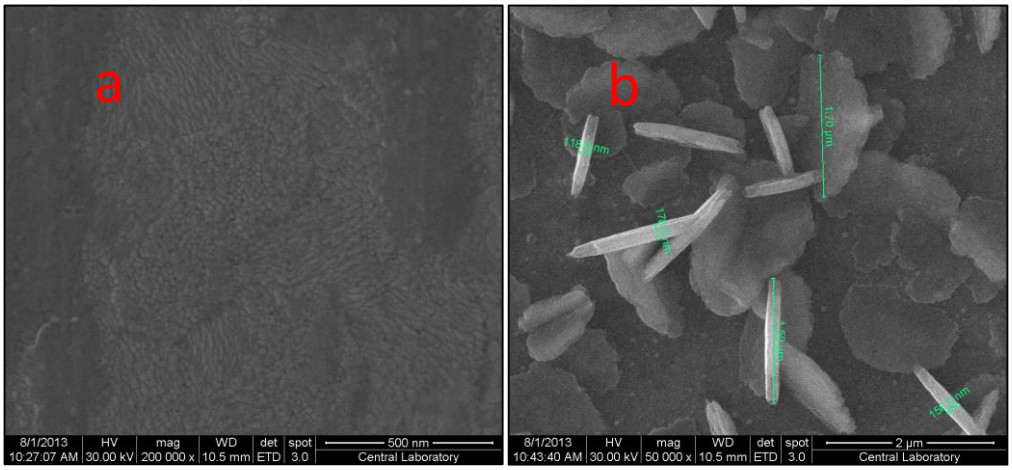

Figure 4.17. SEM image of the sample electrodeposited at 70 °C, a) ZnO, b) ZnO/ V^{+5} , 1.2 VDC for 30 minutes

Similar surface images were obtained for the samples electrodeposited at 70 °C and dip coated with the aqueous solution of NH_4VO_3.

4.1.3. Surface Imaging with AFM

Surface morphology of the samples electrodeposited at room temperature and at 70 °C were also studied with AFM in order to observe the effect of synthesis temperature on the deposition rate of ZnO thin films.

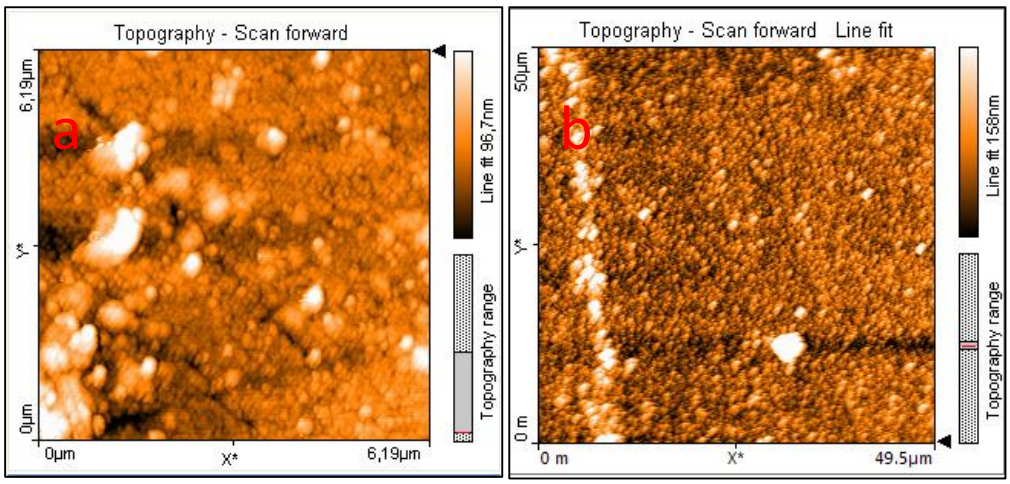

Figure 4.18. AFM images of ZnO thin film samples electrodeposited at a) room temperature, b) 70 °C

Figure 4.18 shows the AFM images of ZnO thin film samples electrodeposited at room temperature and 70 °C, respectively. SEM images can give more detailed information about the morphology of the thin films before and after dip coating with vanadium and the content can be determined by EDAX, whereas, in these samples, AFM images show the difference of the deposition rate at different temperatures. The difference of the roughness of ZnO thin films electrodeposited at room temperature and at 70 °C proves that the deposition rate at 70 °C is higher than the deposition rate at room temperature, because the surface of the sample electrodeposited at room temperature seemed to be smoother than that of the sample electrodeposited at 70 °C. Calculated average area roughness values of the samples within a total area of 2.496 nm^2 are given in Table 4.3.

Table 4.3: Average area roughness values of the samples

Sample	Average Area Roughness (S_a)
Room Temperature	$18{,}644\ nm$
70 °C	$27{,}602\ nm$

4.1.4. X-Ray Diffraction (XRD)

X-Ray Diffraction analysis on zinc oxide thin film calcined at 500 °C was performed in order to determine the crystal structure of the sample.

The crystal structure of the thin films were analyzed by X-Ray diffraction patterns. The X-ray diffractometer was adjusted into angles (2θ) between 20° to 80° with a grazing angle of 0.5° and scanning speed of 1.000 deg/min. The obtained diffractograms were compared with Joint Committee on Powder Diffraction Standards (JCPDS) files. All XRD peaks were assigned according to PDF 01-089-4596 and PDF 036-1451 cards for ITO coated glass substrates and ZnO, respectively.

Figure 4.19 shows the XRD diffractogram of the ZnO thin film sample prepared at room temperature. The thin film was synthesized at room temperature, 4 VDC for 20 hours.

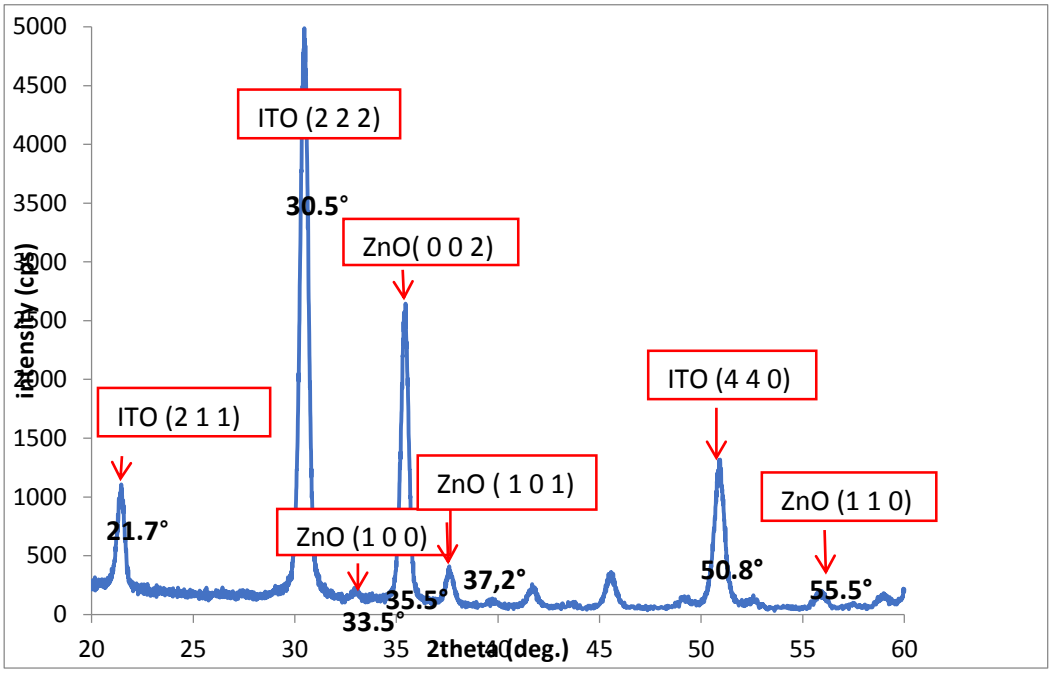

Figure 4.19. XRD pattern of ZnO thin film sample peak positions of ITO coated glass and ZnO, respectively.

The peaks existing at 21.7°, 30.5° and 50.8° degrees show the presence of (2 1 1), (2 2 2) and (4 4 0) planes of indium tin oxide (ITO) phase over amorphous glass sample, respectively. Similarly, the peaks existing at 33.5°, 35.5°, 37.2° and 55.5° degrees show the presence of (1 0 0), (0 0 2), (1 0 1) and (1 1 0) planes of ZnO, respectively.

Crystal structure and orientation of the ZnO thin film were investigated by XRD patterns and the intensity of the peaks relative to the background demonstrates that the sample is highly crystalline. Figure 4.20 indicates that the crystalline ZnO thin film reveal that the existence of a ZnO single phase with a hexagonal wurtzite structure and the XRD pattern consists of a (0 0 2) main peak, indicating that ZnO crystals grew along c- axis.

The difference between the experimental peak position and the reference peak position might be explained by the shift in the settings of the X- Ray diffractometer.

4.1.5. X-Ray Photoelectron Spectroscopy (XPS)

XPS analysis of vanadium doped ZnO thin films at room temperature were performed in order to analyze the O and V species and the oxidation state of vanadium doped on the samples.

Table 4.4. XPS range of fields

	V2p	O1s	Zn2p3	Zn2p1
Energy Interval (eV)	536 – 511	543 – 523	1036-1016	1055-1035

Table 4.4. shows the selected energy fields for XPS analysis.

Survey scan of both of the samples were corrected according to the carbon peak at binding energy of 285 eV and they are given in Figure 4.20.

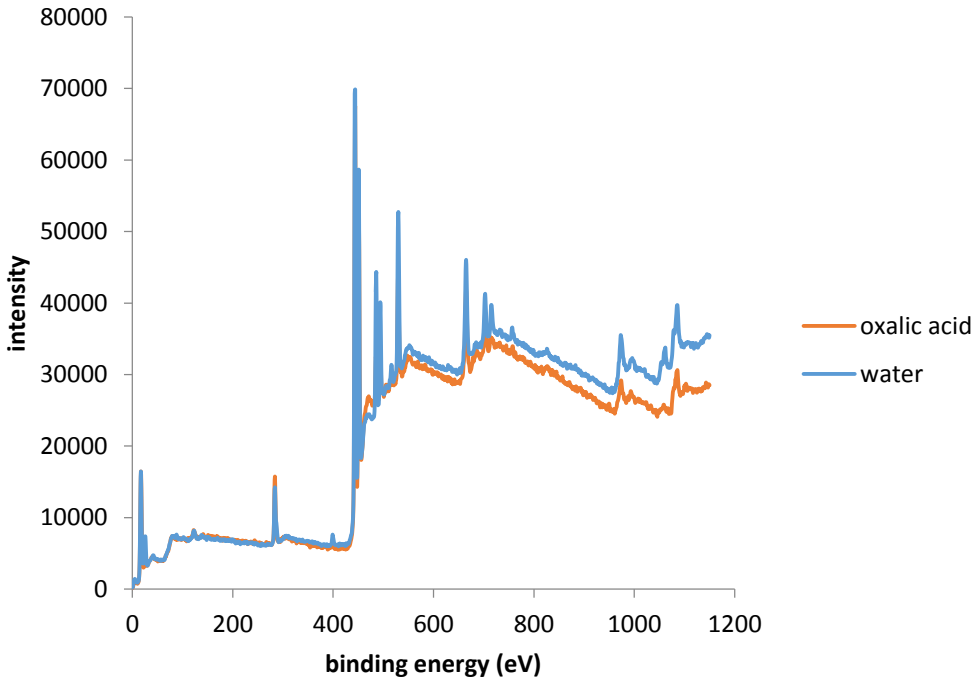

Figure 4.20. XPS survey scan of vanadium doped ZnO thin film samples

Both of the samples were electrodeposited at room temperature during 20 hours, one of them were dip coated with aqueous solution of NH_4VO_3 and the other one was dip coated with NH_4VO_3 solution dissolved in oxalic acid.

Figures 4.21 and 4.22 show the XPS O1s and V2p spectra of the samples, respectively.

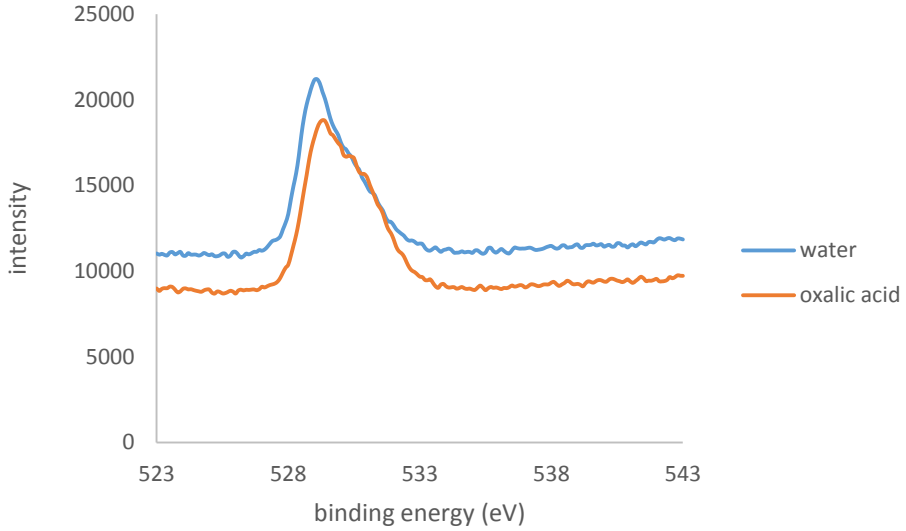

Figure 4.21. XPS O1s spectra of the samples

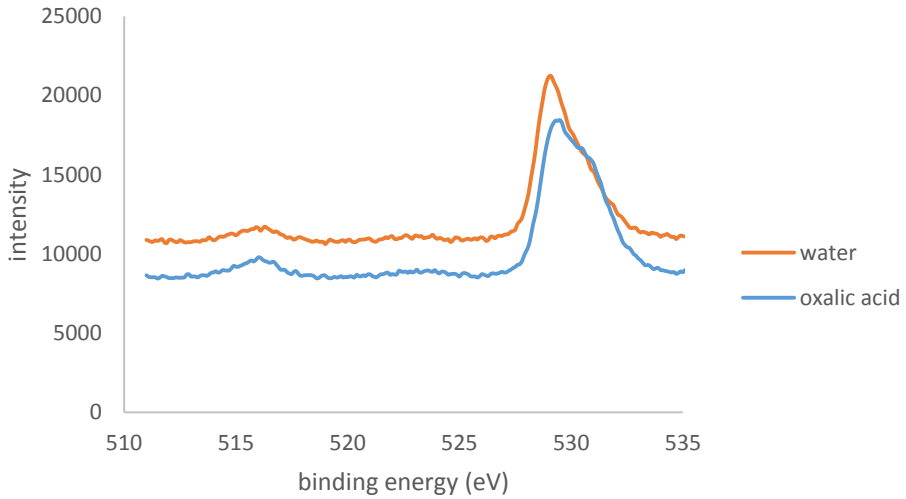

Figure 4.22. XPS V2p spectra of the samples

In order to determine the oxidation state of vanadium in the samples, V2p spectra has been studied in detail. As mentioned before, when NH_4VO_3 is dissolved in water, it gives a pale yellow solution in which the oxidation state of vanadium is (+5) and when NH_4VO_3 is dissolved in aqueous oxalic acid, it gives a dark coloured solution in which the oxidation state of vanadium is (+4) because oxalic acid acts as a reducing agent. Therefore, in order to determine the oxidation state of vanadium, $V^{+5}$and V^{+4}peaks are deconvoluted by using XPS Peak 4.1 software.

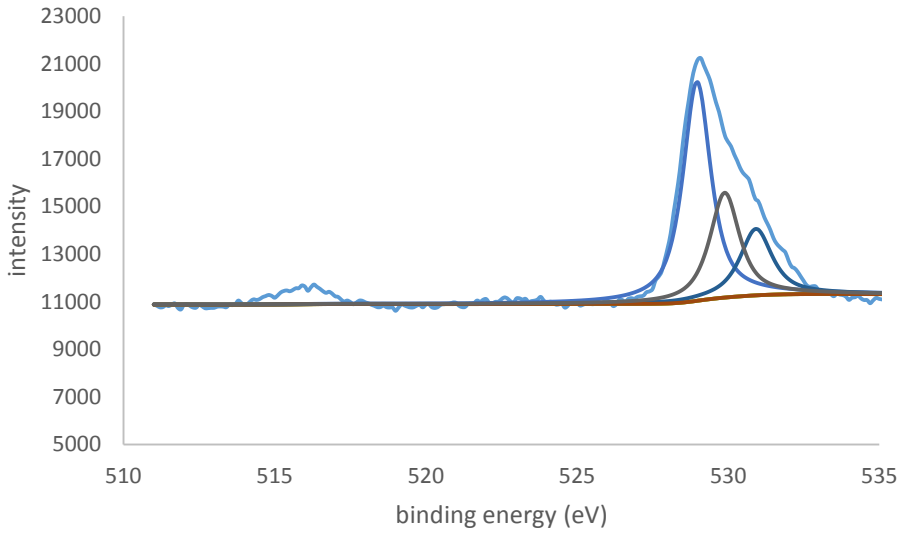

Figure 4.23. XPS O1s spectrum of V-ZnO (+5)

Figure 4.23 shows the deconvoluted XPS O1s spectrum of the sample dip coated with aqueous solution of NH_4VO_3. O1s peaks were observed at 530.9, 529.8 and 528.9 eV for V_2O_5. A $V2p_{3/2}$ peak has also been observed at 517.2 eV for V_2O_5, but the signal to noise ratio of the peak is very low for characterization.

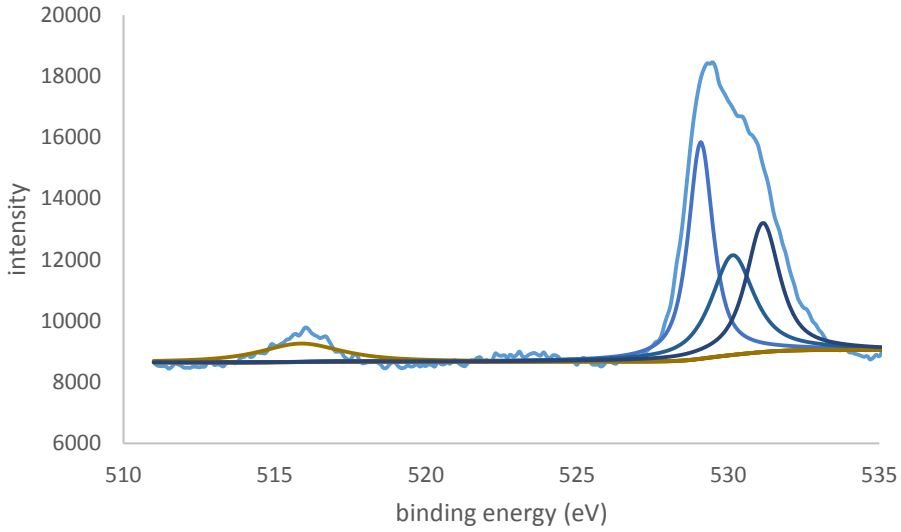

Figure 4.24. XPS O1s spectrum of V-ZnO (+4)

Figure 4.24 shows the XPS O1s spectrum of the sample dip coated with NH_4VO_3 solution where NH_4VO_3 is dissolved in oxalic acid. O1s peaks were observed at 531.1, 529.8, 529 and 515.4 eV for VO_2. $V2p_{3/2}$ peak was also observed near 515.4 eV for VO_2. Similarly to the first sample, the peak observed at 515.4 eV was also small in this sample but it was big enough for

characterizing. XPS spectra of this sample proved that the oxidation state of vanadium here is (+4).

4.2. Photocatalytic Activity Tests

In this part, the photocatalytic activities of the ZnO and V-ZnO thin film samples which are prepared at room temperature and at 70 °C are discussed. The photocatalytic acivity tests were performed by both methylene blue and stearic acid degradation tests.

4.2.1. Methylene Blue Degradation Tests

Methlylene blue degradation method is a common method in order to test the photocatalytic activity of thin film samples. Photocatalytic activity test was performed on V^{+4}, V^{+5} doped and undoped ZnO thin film samples. The experiments performed in two consequitive steps. In the first step, the adsorption of methylene blue on thin film samples were performed by using 20, 50 and 100 ppm methylene blue solutions for 24 hours in dark. After 24 hours, UV-Vis spectra of the samples were obtained to check methylene blue adsorbtion over the samples. The adsorbed methylene blue over thin film samples was tested before the photocatalytic reaction was started. Figure 4.25 gives the methylene blue adsorption spectra of the thin film samples.

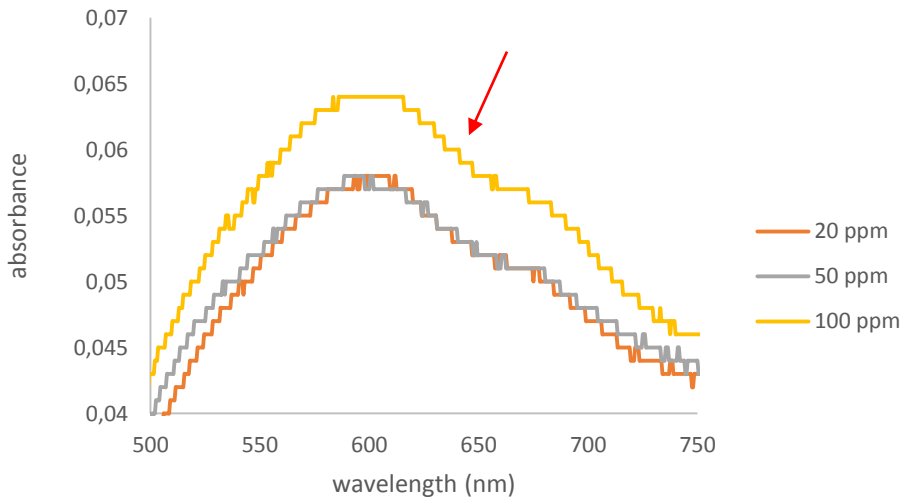

Figure 4.25. MB adsorption spectra of ZnO thin film samples prepared at room temperature,4 VDC for 20 hours

Figure 4.25 shows the MB adsorption spectra of ZnO thin film samples prepared at room temperature during 20 hours. MB peak was obtained near 600-650 nm. Absorbance data indicates the adsorbed amount of MB depends on the initial concentration of MB. Methylene blue dimer peaks were observed near 650 nm. It is reported in literature that the dimerization of MB increases with the concentration [65]. It was also reported that dimerization has a decreasing effect on the degradation rate [5]. In order to avoid dimerization, further experiments were performed with 20 ppm MB solution. Therefore performing MB degradation tests with 100 ppm MB was avoided since 100 ppm was very concentrated for UV-Vis spectrophotometer.

In the second part of the experiments, the photocatalytic degradation of methylene blue adsorbed over ZnO thin film samples was carried out under 300 W/m^2 artificial solar irradiation between 280-780 nm wavelengths. The 30 minute interval time course of the degradation reaction was obtained by measuring the methylene blue concentration over surface. The UV-Vis spectrum of the samples between 200-800 nm was obtained from the same spot of the thin film sample.

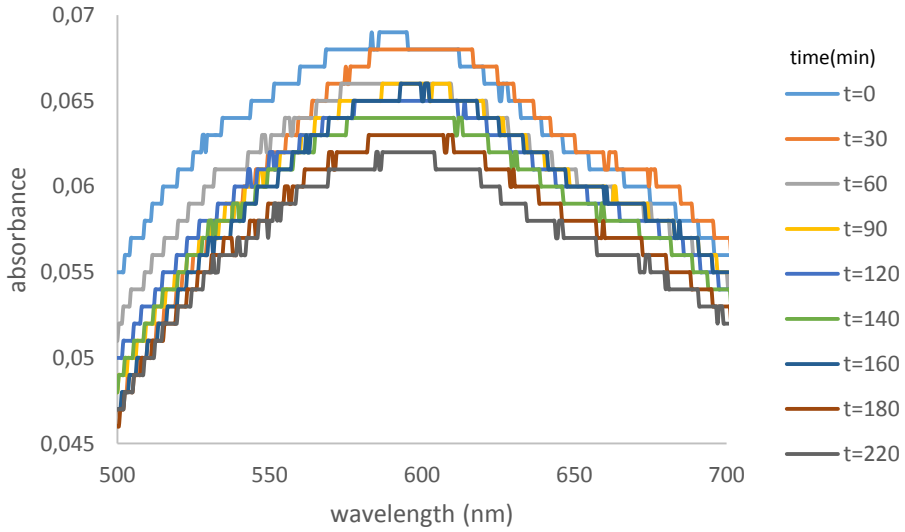

Figure 4.26. UV-Vis spectra of the methylene blue adsorbed ZnO sample irradaiated under 300W/m^2 artificial irradiation.

Figure 4.26 shows the MB degradation plots obtained 30 minute intervals for the sample prepared at room temperature, 4 VDC for 20 hours. Decrease in the absorbance data gives the information about the decrease in the concentration of MB dye adsorbed on the thin film sample, according to the photodecomposition reaction of MB dye or self cleaning activity under solar irradiation. The decrease in the absorbance data proves that the prepared thin films are photocatalytically active.

The photocatalytic activity of the thin film samples were also determined for liquid phase degradation of methylene blue. For this purpose, the liquid phase UV-Vis spectrum of methylene blue was analyzed first to determine the wavelenght which the corresponding absorbance has a linear relationship with methylene blue concentration. The UV-Vis spectrum of 3 ppm MB solution is given in Figure 4.27. According to the spectrum, the wavelength, where the maximum peak is obtained was determined as 664,5 nm. Then the spectrophotometer was set to 664,5 nm and absorbance data of the samples were obtained at 664,5 nm.

Decomposition studies proved that the thin film samples were photocatalytically active.

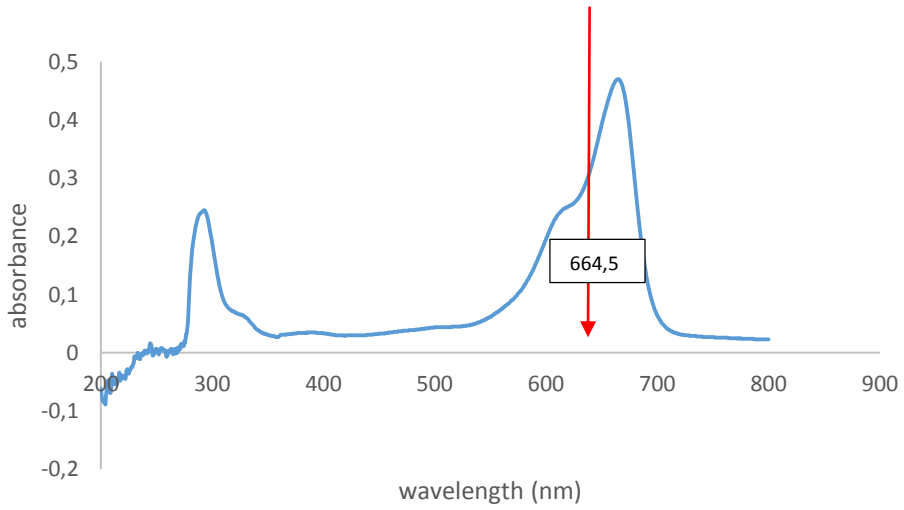

Figure 4.27. UV-Vis spectrum of 3 ppm MB solution

The photocatalytic activities of thin films for aqueous phase methylene blue were determined by using 6 ml of 3 ppm MB solution in petri dishes. The distance between the light source and the petri dishes was set as 5 cm. In this set of experiment, 254 nm, 15 watt UV lamps are used as light source. The sample prepared at room temperature, 4 VDC for 20 hours was immersed into solution and exposed to UV light. The time course of reaction was obtained by measuring methylene blue concentration in solution. The results are compared with the photodegradation of methylene blue. For this purpose, the blank experiments were performed by exposing the same amount of methylene blue solution in petri dishes without thin film samples. The same procedure was applied to other samples prepared at 70 °C. The results are presented in Figures 4.28 and 4.29.

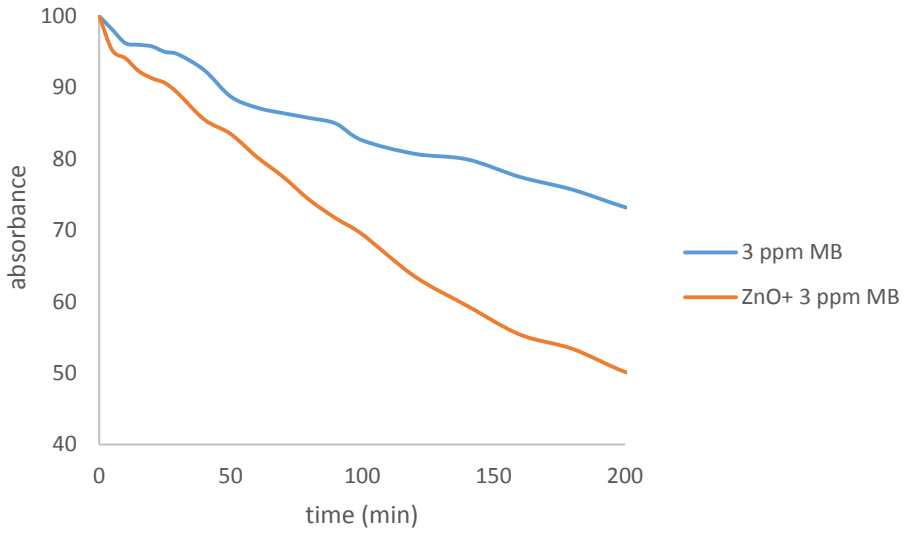

Figure 4.28. MB degradation of the ZnO thin film sample prepared at room temperature,4 VDC for 20 hours

Figures 4.28 and 4.29 show the MB degradation results of the samples prepared at room temperature and 70 °C. Before discussing the results of these experiments, the effect of ZnO thin film can be clearly seen from both of the figures, the degradation of MB dye is more in the presence of ZnO thin film.

According to figure 4.28, MB dye degraded 37 % in the absence of ZnO thin film. This result increased to 50 % degradation in the presence of ZnO thin film within 160 minutes.

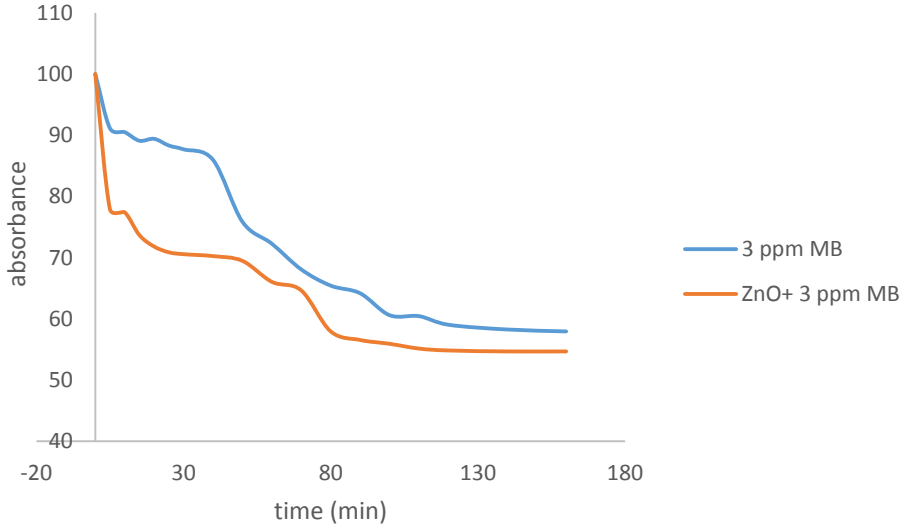

Figure 4.29. MB degradation for the sample prepared at 70 °C

Figure 4.29 shows the results of the sample prepared in 70 °C. The degradation of MB dye was observed as 43% and 46% in the absence and presence of ZnO thin film, respectively. This experiment lasted 160 minutes.

The photocatalytic activity of samples prepared at 70°C are unexpectidely lower than samples prepared at room temperature. At the end of 160 minutes, the thin film sample deposited at room temperature, 50% degradation was obtained. However, 46% conversion was obtained by using sample prepared at 70°C. The formation of dense layer of thin film may result with lower activity.

Similarly, the effect of vanadium doping on the photocatalytic activity of thin film samples were determined. For this purpose, the photocatalytic activities of V^{+4} and V^{+5} doped ZnO thin film sample prepared at 70 °C were tested and the results were compared with bare ZnO thin film sample. This experiment was performed under 300 W/m^2 artificial solar irradiation between 280-780 nm with the same procedure of the former experiment. The results of the experiments are shown in Figure 4.30.

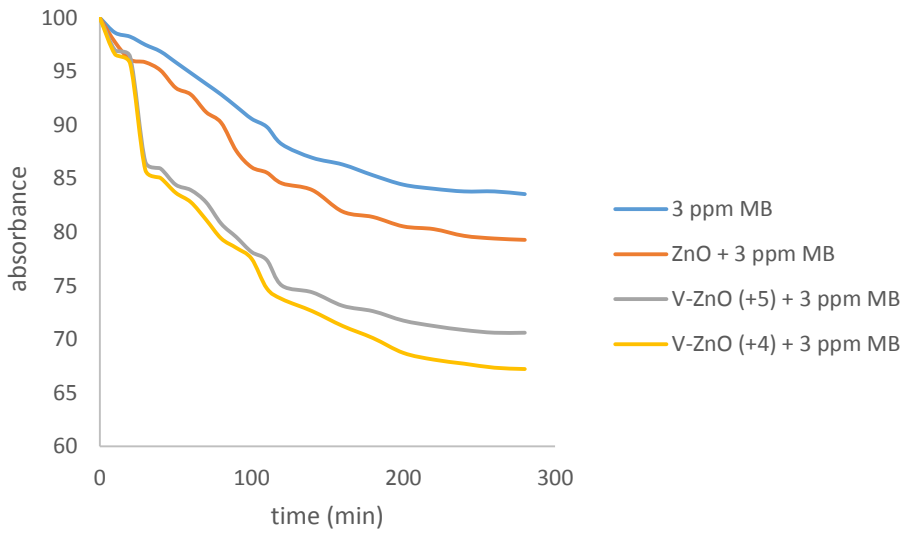

Figure 4.30. MB degradation results and the effect of vanadium doping on ZnO samples prepared at 70 °C, 1.2 VDC for 30 minutes

Under 300 W/m^2 artificial solar irradiation, 17% conversion at the end of 280 minutes was obtained for the photodegradation of methylene blue. The presence of ZnO thin film increased the degradation to 20 % at the percent. The V^{+4} and V^{+5} doped samples performed better and highest activity was observed for V^{+4} doped sample as 33 % conversion. Thus, vanadium

doping significantly enhance the photocatalytic activity of ZnO thin films and V^{+4} doped ZnO sample has higher activity for methylene blue degradation reaction.

4.2.2. Stearic Acid Degradation Tests

Stearic acid degradation tests also performed in order to obtain more information about the photocatalytic activity of ZnO and vanadium doped ZnO thin film samples.

ZnO, and V^{+4} and V^{+5} doped samples prepared at room temperature by electrodepositon, 4 VDC potential for 20 hours were dip coated with 40 mg/L stearic acid solution. Thin film samples were exposed to 36 W, 254 nm UV lamp. Then, the photocatalytic decomposition of stearic acid on the thin film samples were monitored by the difference in the asyymmetric C-H streching modes of CH_3 groups and the symmetric- asymmetric C-H streching modes of CH_2 groups in the region 2700-3000 cm^{-1} FT-IR spectra.

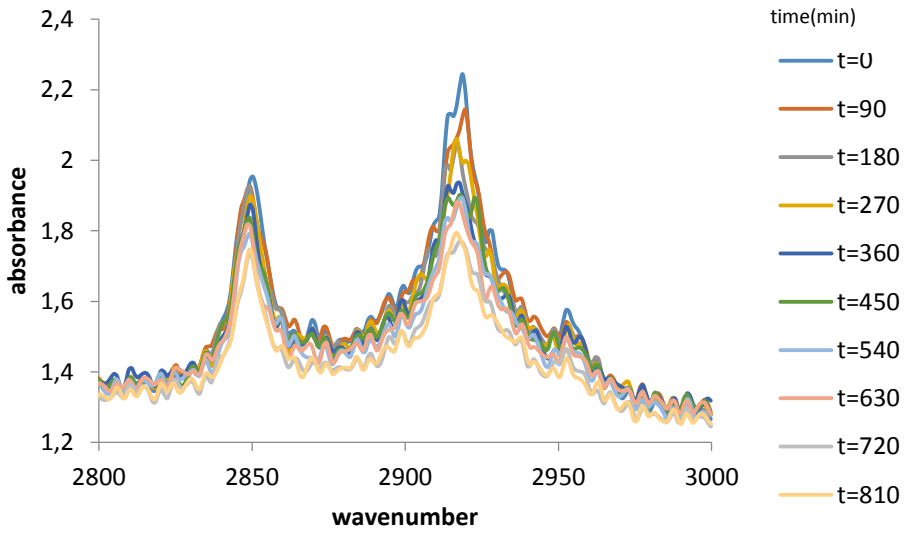

Figure 4.31. FT-IR spectra of the degradation of stearic acid on ZnO thin film

Figure 4.31 shows the time course of FT-IR absorption spectra of stearic acid film over ZnO thin film and the change of absorbance corresponding to C-H streching peaks with respect to time. The maximum absorbance values of the peaks were obtained at 2918 and 2849 cm^{-1}. The fractional conversion for stearic acid degradation reaction was obtained from the absorbance values. The percent conversion of stearic acid was calculated as 22% at the end of 810 minutes (Figure 4.32)

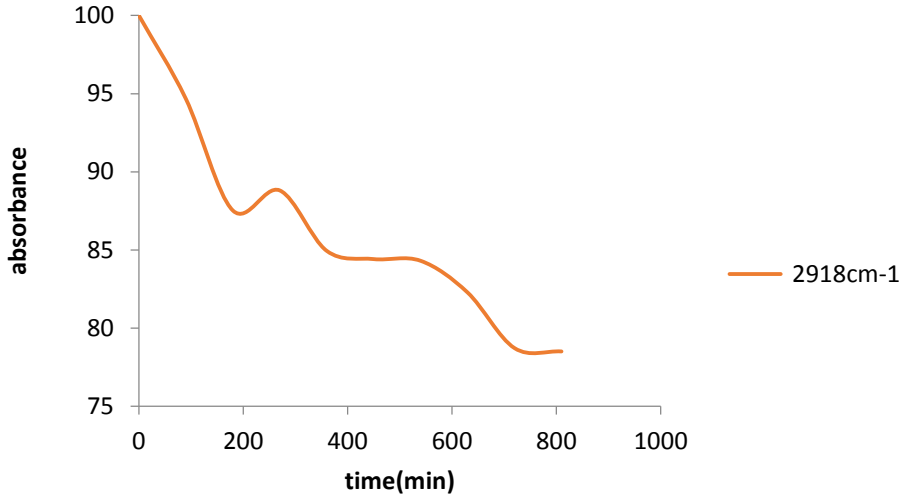

Figure 4.32. Conversion % of stearic acid on ZnO thin film sample

According to Figure 4.32, conversion percent of stearic acid in wavenumber 2918 cm^{-1} was obtained as 22%.

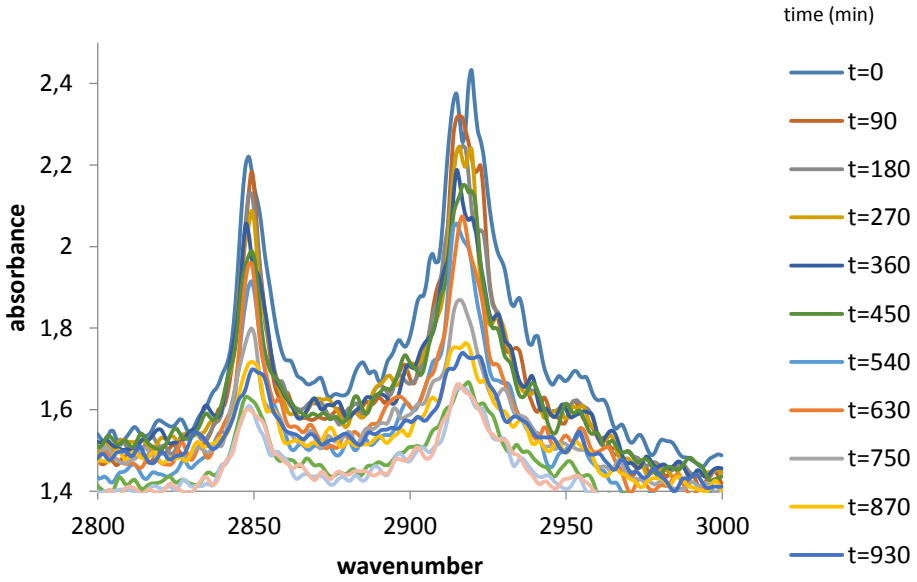

Figure 4.33. FT-IR spectra of the degradation of stearic acid on V^{+5} doped ZnO thin film

Figure 4.33 demonstrates the FT-IR absorbance spectra of the degradation of stearic acid over V^{+5} doped ZnO thin film sample. The maximum peaks were obtained at 2918 and 2849 cm^{-1}

and the conversion percent of stearic acid was calculated from the decrease of the absorbance data obtained in 2918 and 2849 cm^{-1}, respectively.

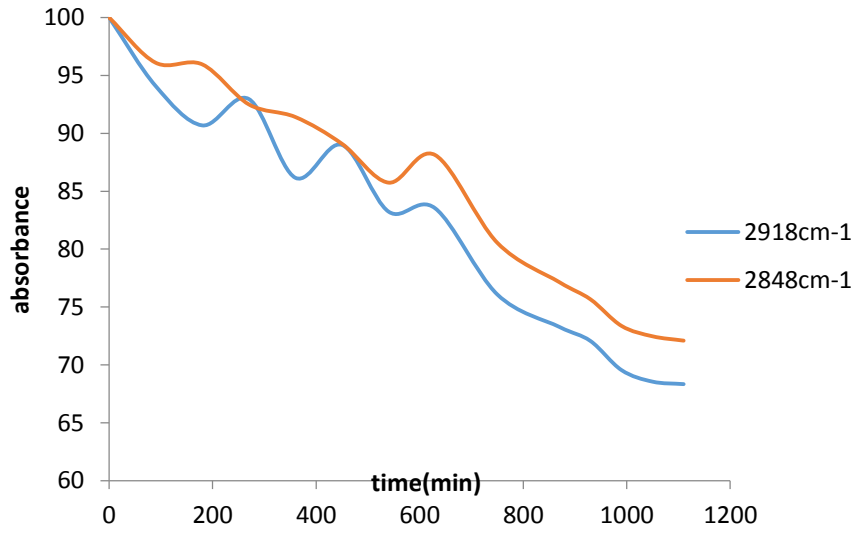

Figure 4.34 Conversion % of stearic acid on V^{+5} doped ZnO thin film sample

Percent conversion of stearic acid over V^{+5} doped ZnO thin film sample was obtained as 32% at the end of 1100 minutes.

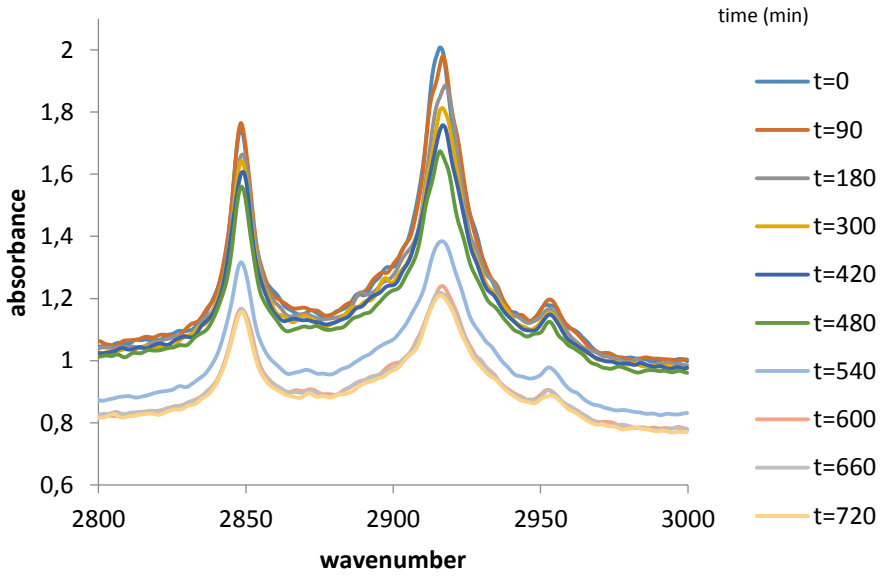

Figure 4.35. FT-IR spectra of the degradation of stearic acid on V^{+4} doped ZnO thin film

Figure 4.35 demonstrates the FT-IR absorbance spectra of the degradation of stearic acid over V^{+4} doped ZnO thin film sample. V^{+4} doped ZnO sample performed better than V^{+5} doped counterpart and 40% conversion was obtained at the end of 720 minutes (Figure 4.36)

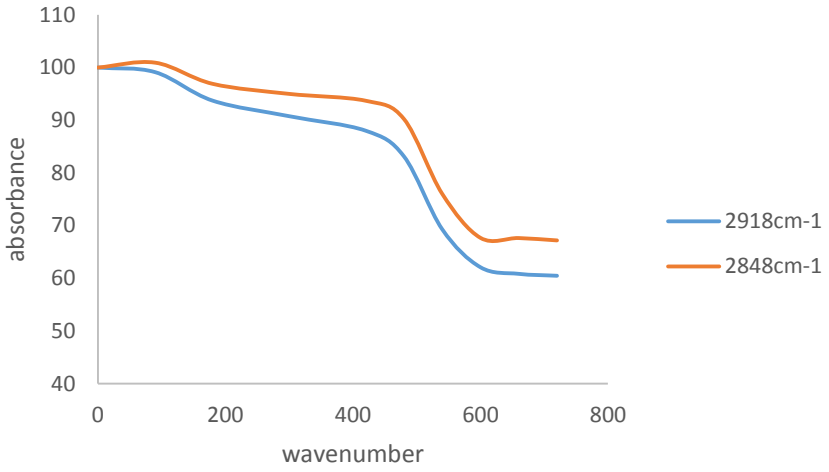

Figure 4.36. Percent conversion of stearic acid over V^{+4} doped ZnO sample

Similar to methylene blue degradation results, the highest photocatalytic activity was obtained over V^{+4} doped ZnO thin film. Photocatalytic activity was followed by V^{+5} doped ZnO thin film and the lowest activity was observed in pure ZnO thin film. These results show that vanadium doping significantly improves the photocatalytic activity of ZnO thin films.

CHAPTER 5

CONCLUSIONS

In this study, photocatalytically active ZnO thin films coated on ITO glass sheets were prepared by electrodeposition method. Synthesis of thin film samples was performed at both room temperature and at 70 °C. In order to investigate the effect of transition metal doping on the photocatalytic activity of ZnO thin films, some samples were dip coated by NH_4VO_3 solutions in which NH_4VO_3 was dissolved in water and oxalic acid. The oxidation state of vanadium in these solutions were expected to be (+5) and (+4), respectively.

Band gap calculations of the thin film samples were calculated by using the absorbance data of the samples obtained between 200- 800 nm in UV- Vis region. Characterization of thin film samples were performed by AFM, SEM, XRD and XPS analysis. Also, elemental composition of the samples was determined by EDX analysis. Photocatalytic activity of the samples were tested by methylene blue and stearic acid degradation reactions. Methylene blue degradation tests were examined by obtaining the absorbance data between 200-800 nm by UV- Vis spectrophotometer. Stearic acid degradation tests were examined by monitoring the difference in the asymmetric C-H streching modes of CH_3 groups and the symmetric- asymmetric C-H streching modes of CH_2 groups in the region 2700-3000 cm^{-1} by FT- IR spectrophotometer.

Methylene blue and stearic acid degradation test results showed that the photocatalytic activity was favored by synthesis temperature, samples prepared at 70 °C showed higher photocatalytic activity than that of the samples prepared at room temperature. Degradation test results indicated that vanadium doping improved the photocatalytic activity. Oxidation state of vanadium also had an effect on the photocatalytic activity of the thin films. Thin film samples dip coated with the solution in which NH_4VO_3 was dissolved in oxalic acid showed higher photocatalytic activity. Photocatalytic activity teste were also performed under different light sources having different light intensities, and it was observed that the intensity of light also had an effect on the degradation rate.

Electrodeposition rate increases with increasing temperature, samples prepared at 70 °C contained higher amounts of zinc on the surface according to EDX analysis. This result was also proved by the AFM images, the surfaces of the samples prepared at 70 °C seemed to be more rough, according to the higher amount of zinc deposited on the surface.

The effect of temperature on the morphology of the thin films was observed by SEM images. Samples prepared at room temperature had uniform surfaces, ZnO was in spherical shape. Increase in temperature increased the deposition rate but the surfaces of the samples prepared at 70 °C was not uniform and ZnO was observed in the nanoplate form and bulk form in the different spots of the same sample. It was also observed that vanadium was not coated on the surface homogenously. This is mostly according to the very slight solubility of NH_4VO_3, NH_4VO_3 might not be homogenously dispersed in the solution although it was stirred at high rpms.

Crystallinity of the samples was investigated by X-Ray diffractometer. The oxidation state of vanadium on the samples was determined by XPS analysis. Vanadium was expected to be in (+5) and in (+4) oxidation state in the solutions, in which NH_4VO_3 was dissolved in water and in oxalic acid, respectively. O1s peaks for V_2O_5 was observed in the XPS spectra of the former sample, but $V2p_{3/2}$ peak was very small for characterizing. Both O1s and $V2p_{3/2}$ peaks for VO_2 were observed in the XPS spectra of the latter sample and they were big enough for characterizing, indicating the the oxidation state of vanadium was (+4) in the latter solution.

REFERENCES

[1] Erkan, A., "Investigation of Thin Semiconductor Coatings and Their Antimicrobial Properties", MSc Thesis, 2005, Ankara.

[2] Kurbanoğlu, B., "Dynamic Resistivity Behavior of Tin Oxide Based Multilayer Thin Films Under Reducing Conditions", MSc Thesis, 2006, Ankara.

[3] Severcan, I., " Dynamic Resistivity Behavior of Tin Oxide Based Thick Films Under Reducing and Oxidizing Conditions", MSc Thesis, 2002, Ankara.

[4] Kondarides, I. D., "Photocatalysis", Encyclopedia of Life Support Systems", Catalysis.

[5] Doğu, D., "The Photocatalytic Activity of Praseodymium Doped Titanium Dioxide", PhD Thesis, 2012, Ankara.

[6] Gadzhiev, G. G., " The Thermal and Elastic Properties of Zinc Oxide- Based Ceramics at High Temperatures", High Temperature, 41, 2003.

[7] Auer, G., Griebler, W. D., Jahn, B., "Industrial Inorganic Pigments", Wiley- VCH Verlag GmbH & Co., 3rd Edition, 2005.

[8] Korkmaz Erdural, B., " Photocatalytic Antimicrobial and Self- Cleaning Properties of Titania- Silica Mixed Oxide Thin Films", PhD Thesis, 2012, Ankara.

[9] Hoffman, M. R., Martin, S. T., Choi, W., Bahnemann, D. W., "Environmental Applications of Semiconductor Photocatalysis, Chemistry Reviews, 95, 1995.

[10] Linsebigler, A. L., Lu, G., Yates, Jr., J. T., " Photcatalysis on TiO_2 Surfaces: Principles, Mechanisms and Selected Results", Chemistry Reviews, 95, 1995.

[11] Mills, A., Hunte Le, S., " An Overview of Semiconductor Photocatalysis", Journal of Photochemistry and Photobiology, 108, 1997.

[12] Fox, M. A., Dulay, M. T., "Heterogenous Photocatalysis", Chemical Reviews, 93, 1993.

[13] Xie, J., Wang, H., Duan, M., Zhang, L., " Synthesis and Photocatalysis Properties of ZnO Structures with Different Morphologies via Hydrothermal Method", Applied Surface Science, 257, 2011.

[14] Soltaninezhad, M., Aminifar, A., " Study Nanostructures of Semiconductor Zinc Oxide (ZnO) as a Photocatalyst for the Degradation of Organic Pollutants", International Journal of Nano dimension, 2, 2011.

[15] Xu, F., Zhang, P., Navrotsky, A., Yuan, Z. Y., Ren, T. Z., Halasa, M., "Hierarchically Assembled Porous ZnO Nanoparticles: Synthesis, Surface Energy and Photocatalytic Activity", Chemistry of Materials, 19, 2007.

[16] Baruah, S., Pal, S. K., Dutta, J., "Nanostructured Zinc Oxide for Water Treatment", Nanoscience& Nanotechnology, Asia, 2, 2012.

[17] Hashimoto. K., Irie., H., Fujishima, A., "TiO_2 Photocatalysis: A Historical Overview and Future Prospects", Japanese Journal of Applied Physics, Vol. 44, No. 12, 2005.

[18] Liao., D. L., Badour, C. A., Liao, B. Q., "Preparation of Nanosized TiO_2/ ZnO Composite Catalyst and its Photocatalytic Activity for Degradation of Methyl Orange", Journal of Photochemistry and Photobiology A: Chemistry, 194, 2008.

[19] Zhu, Y. F., Xu, S. B., Yi, D., "Photocatalytic Degradation of Methyl Orange Using Polythiophene/ Titanium Dioxide Composites", Reactive and Functional Polymers, 70, 2010.

[20] Ni, M., Leung, M. K. H., Leung, Y. C. D., Sumathy, K., " A Review and Recent Developments in Photocatalytic Water Splitting Using TiO_2 for Hydrogen Production", Renewable and Sustainable Energy Reviews, 11, 2007.

[21] Arya, S. K., Saha, S., Ramirez-Vick J. E., Gupta, V., Bhansali, S., Singh, S.P., "Recent Advances in ZnO Nanostructures and Thin Films for Biosensor Applications: Review", Analytica Chimica Acta, 737, 2012.

[22] Janotti, A., Van de Walle, C., "Fundamentals of Zinc Oxide as a Semiconductor", Reports on Progress in Physics, 72, 2009.

[23] Haffad, S., Cicero, G., Samah, M., "Structural and Electronic Properties of ZnO Nanowires: A Theoritical Study", Energy Procedia, 10, 2011.

[24] Moezzi, A., McDonagh, A. M., Cortie, M. B., " Zinc Oxide Particles: Synthesis, Properties and Applications", Chemical Engineering Journal, 185-186, 2012.

[25] Özgür, Ü., Alivov, Y. I., Liu, C., Teke, A., Reshchikov, M. A., Doğan, S., Avrutin, V., Cho, S. J., Morkoç, H., "A Comprehensive Review of ZnO Materials and Devices", Journal of Applied Physics, 98, 2005.

[26] Djurisic, A. B., Ng, A. M. C., Chen, X. Y., "ZnO Nanostructures for Optoelectronics: Material Properties and Device Appliations", Progress in Quantum Electronics, 34, 2010.

[27] Krebs, H. U., Weisheit, M., Faupel, J., Süske, E., Scharf, T., Fuhse, C., Störmer, M., Sturm, K., Seibt, M., Kijevski, H., Nelke, D., Panchenko, E., Buback, M., "Pulsed Laser Deposition (PLD) – a Versatile Thin Film Technique", Applied Surface Sciences, 462, 2000.

[28] Sun, X. W., Kwok, H. S., "Optical Properties of Epitaxially Grown Zinc Oxide Thin Films on Sapphire by Pulsed Laser Deposition", Journal of Applied Physics, 86, 1999.

[29] Vinodkumar, R., Lethy, K. J., Beena, D., Detty, A. P., Navas, I., Nayar, U. V., Pillai Mahadevan, V. P., Ganesan, V., Reddy, V. R., "Effect of ITO Buffer Layers on the Structural, Optical and Electrical Properties of ZnO Multilayer Thin Films Prepared by Pulsed Laser Deposition Technique, Solar Energy Materials & Solar Cells, 94, 2010.

[30] Triboulet, R., Perriére, J., " Epitaxial Growth of ZnO Films", Progress in Crystal Growth and Characterization of Materials, 47, 2003.

[31] Park, J. H., Muralidharan, P., Kim, D. K., " Solvothermally Grown ZnO Nanorod Arrays on (101) and (002) Single- and Poly- Crystalline Zn Metal Substrates", Materials Letters, 63, 2009.

[32] Mouet, T., Devers, T., Telia, A., Messai, Z., Harel, V., Konstantinov, K., Kante, I., Ta, M. T., " Growth and Characterization of Thin ZnO Films Deposited on Glass Substrates by Electrodeposition Technique", Applied Surface Science, 256, 2010.

[33] Willander, M., Nur, O., Zhao, Q. X., Yang, L. L., Lorenz, M., Cao, B. Q., Zuniga Pérez, J., Czekalla, C., Zimmermann, G., Grundmann, M., Bakin, A., Behrends, A., Al- Suleiman, M., El- Shaer, A., Che Mofor, A., Postels, B., Waag, A., Boukos, N., Travlos, A., Kwack, H. S., Guinard, J., Dang, D. L. S., "Zinc Oxide Nanorod Based Photonic Devices: Recent Progress in Growth, Light Emitting Diodes and Lasers", Nanotechnology, 20, 2009.

[34] Zhang, L., Chen, Z., Tang, Y., Jia, Z., " Low Temperature Cathodic Electrodeposition of Nanocrystalline Zinc Oxide Thin Films", Thin Solid Films, 492, 2005.

[35] Machado, G., Guerra, D. N., Leinen, D., Ramos- Barrado, J. R., Marotti, R. E., Dalchiele, E. A., " Indium Doped Zinc Oxide Thin Films Obtained by Electrodeposition", Thin Solid Films, 490, 2005.

[36] Elias, J., Tena- Zaera, R., Lévy- Clement, C., "Effect of the Chemical Nature of the Anions on the Electrodeposition on ZnO Nanowire Arrays", Journal of Physical Chemistry, 112, 2008.

[37] Mirkelamoğlu, B., "Investigation of Carbon Monoxide Oxidation over Tin Dioxide Based Catalysts by Dynamic Methods", MSc Thesis, 2002, Ankara.

[38] Fraden, J., "Handbook of Modern Sensors, Physis, Design and Applications", United Book Press Inc., 1996, 2nd Edition.

[39] Inamdar, A. I., Sonavane, A. C., Sharma, S. K., Hyunsik Im, Patil, P.S., "Nanocrystallite zinc oxide thin films by novel double pulse single step electrodeposition", Journal of Alloys and Compounds, 495, 2010.

[40]Michaelis, E., Wöhrle, D., Rathousky, J., Wark, M., "Electrodeposition of porous zinc oxide electrodes in the presence of sodium laurylsulfate", Thin Solid Films, 497, 2006.

[41]Yeo, K. H., Teh, L. K., Wong, C. C. "Process and characterization of macroporous periodic nanostructured zinc oxide via electrodeposition", Journal of Crystal Growth, 287, 2006.

[42]Inamdar, A.I., Mujawar, S. H., Sadale, S. B., Sonavare, A. C., Shelar, M. B., Shinde, P. S., Patil, P. S., "Electrodeposited zinc oxide thin films: Nuleation and growth mechanism", Solar Energy Materials and Solar Cells, 91, 2007.

[43] Fan, Z., Lu, J. G., "Zinc Oxide Nanostructures: Synthesis and Properties", Journal of Nanoscience and Nanotechnology, 5, 2005.

[44] Porter, F. C., "Zinc Handbook: Properties, Processing and Use in Design", Taylor & Francis, 1991.

[45] Yassıtepe, E., Yatmaz, H. C., Öztürk, C., Öztürk, K., Duran, C., "Photocatalytic Efficiency of ZnO Plates in Degradation of Azo Dye Solutions", Journal of Photochemistry and Photobiology A: Chemistry, 198, 2008.

[46] Sobana, N., Swaminathan, M., "The Effect of Operational Parameters on the Photocatalytic Degradation of Acid Red 18 by ZnO", Separation and Purification Technology, 56, 2007.

[47] Chakrabarti, S., Dutta, B. K., "Photocatalytic Degradation of Model Textile Dyes in Wastewater Using ZnO as Semiconductor Catalyst", Journal of Hazardous Materials, B112, 2004.

[48] Dijken, A. V., Janssen, A. H., Smitsmans, M. H. P., Vanmaelkelbergh, D., Meijerink, A., "Size- Selective Photoetching of Nanocrystalline Semiconductor Particles", Chemistry of Materials, 10, 1998.

[49] Bickley, R. J., Stone, F. S., "Photoadsorption and Photocatalysis at Rutile Surfaces: I. Photoadsorption of Oxygen", Journal of Catalysis, 31, 1973.

[50] Gaya, U. I., Abdullah, A. H., "Heterogenous Photocatalytic Degradation of Organic Contaminants over Titanium Dioxide: A Review of Fundamentals, Progress and Problems, " Journal of Photochemistry and Photobiology, 9, 2008.

[51] Chen, D., Sivakumar, M., Ray, A. K., "Heterogenous Photocatalysis in Environmental Remedation", Developments in Chemical Engineering and Mineral Processing, 8, 2000.

[52] Alvarez, P. J., Colvin, V., Lead, J., Stone, V. A. N., "Research Priorities to Advance Eco-Responsible Nanotechnology", ACS Nano, 3, 2009.

[53] Ghazzal, M. N., Barthen, N., Chaoui, N., "Photodegradation Kinetics of Stearic Acid on UV- Irradiated Titania Thin Film Seperately Followed by Optical Microscopy and Fourier Transform Infrared Spectroscopy", Applied Catalysis B: Environmental, 103, 2011.

[54] Sunada, K., Kikuchi, Y., Hashimoto, K., Fujishima, A., " Bactericidal and Detoxification Effects of TiO_2 Thin Film Photocatalysts", Environmental Science and Technology, 32, 1998.

[55] Haber, J., Witko, M., Tokarz, R., " Vanadium Pentoxide I. Structures and Properties", Applied Catalysis A: General", 157, 1997.

[56] Chain, E. E., "Optical properties of vanadium dioxide and vanadium pentoxide thin films", Applied Optics, 30, 1991.

[57] Weckhuysen, B. M., Keller, D. E., "Chemistry, spectroscopy and the role of supported vanadium oxides in heterogenous catalysis", Catalysis Today, 78, 2003.

[58] Wokaun, A., Schraml, M., " Characterization of Vanadia/ Silica Mixed Gel Catalysts by Vibrational Spectroscopy", Journal of Catalysis, 116, 1989.

[59] Kazunori, S., Hiroshi, K. Y.," Material design for transparent ferromagnets with ZnO-based magnetic semiconductors", Japanese Journal of Applied Physics, 39, 2000.

[60] Tahir, N., Hussain, S. T., Usman, M., Hasanain, S. K., Mumtaz, A., "Effect of vanadium doping on structural, magnetic and optical properties of ZnO nanoparticles", Applied Surface Sciences, 255, 2009.

[61] Koleva, M. E., Atasanov, P. A., Nedialkov, N. N., Fukuoka, H., Obara, M., "Role of vanadium content in ZnO thin films grown by pulsed laser deposition", Applied Surface Sciences, 254, 2007.

[62] Krithiga, R., Chandrasekaran, G., "Synthesis, structural and optical properties of vanadium doped zinc oxide nanograins", Journal of Crystal Growth, 311, 2009.

[63] Patil S.L., Chougule M.A., Pawar S.G., Raut S.G., Sen S., Patil V.B., ''New process for synthesis of ZnO thin films: microstructural, optical and electrical characterization'', Journal of Alloys and Compounds, 509, 2011.

[64] Lupan, O., Guérin, V. M., Tiginyanu, I. M., Ursaki, V. V., Chow, L., Heinrich, H., Pauporté, T., "Well- aligned arrays of vertically oriented ZnO nanowires electrodeposited on ITO- coated glass and their integration in dye sensitizied solar cells", Journal of Photochemistry and Photobiology A: Chemistry, 211, 2010.

[65] Jockusch, S., Turro, N. J., "Aggregation of methylene blue adsorbed on starburst dendrimers", Macromolecules, 28, 1995.

APPENDIX A

ENERGY DISPERSIVE X-RAY (EDX) ANALYSIS RESULTS

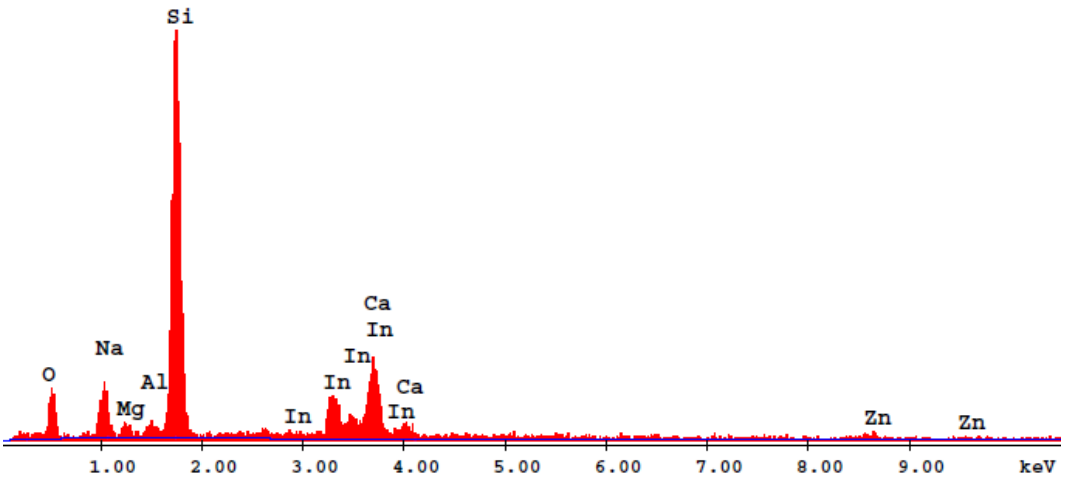

Figure A.1: EDX analysis of ZnO thin film sample electrodeposited at room temperature

Table A.1: EDX quantification table of ZnO thin film sample electrodeposited at room temperature

Element	Wt %	At %
O	22.07	36.79
Na	10.01	11.61
Mg	2.19	2.40
Al	1.57	1.56
Si	40.14	38.11
In	13.63	3.17
Ca	8.27	5.51
Zn	2.11	0.86
Total	100.00	100.00

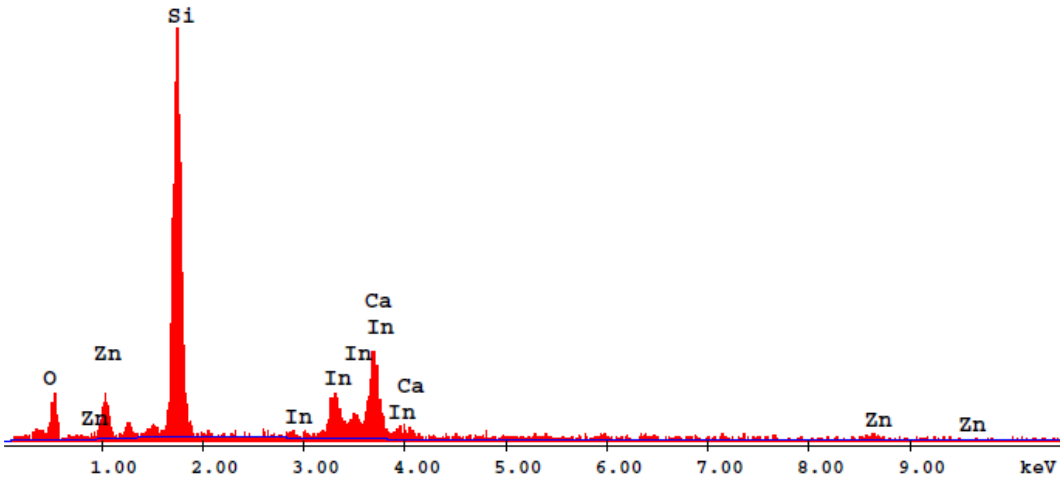

Figure A.2: EDX analysis of ZnO thin film sample electrodeposited at 70 °C

Table A. 2: EDX quantification table of ZnO thin film sample electrodeposited at 70 °C

Element	Wt %	At %
O	26.63	45.35
Si	43.86	42.55
In	16.58	3.93
Ca	10.56	7.18
Zn	2.36	0.99
Total	100.00	100.00

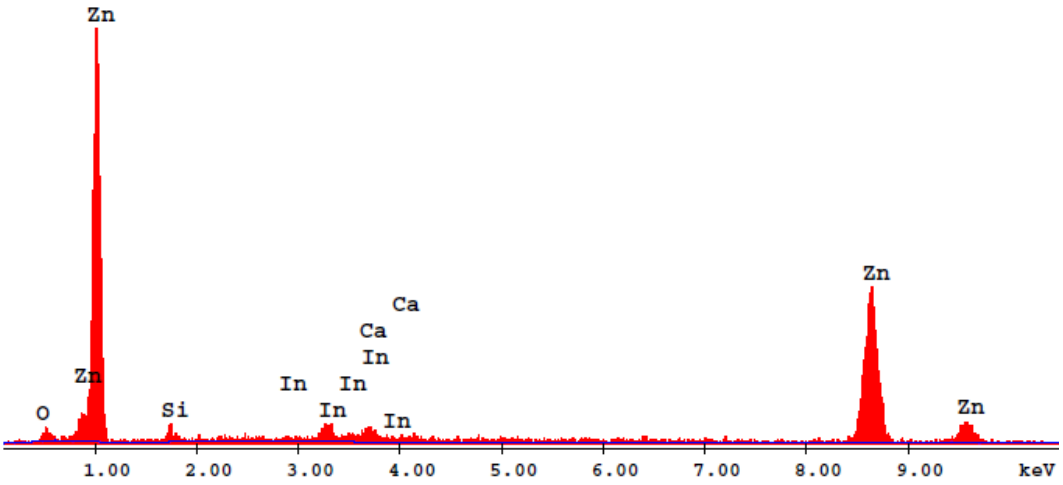

Figure A.3: EDX analysis of ZnO thin film sample electrodeposited at 70 °C

Table A.3: EDX quantification table of ZnO thin film sample electrodeposited at 70 °C

Element	Wt %	At %
O	5.46	18.47
Si	4.32	8.32
In	7.23	3.40
Ca	2.24	3.02
Zn	80.75	66.79
Total	100.00	100.00

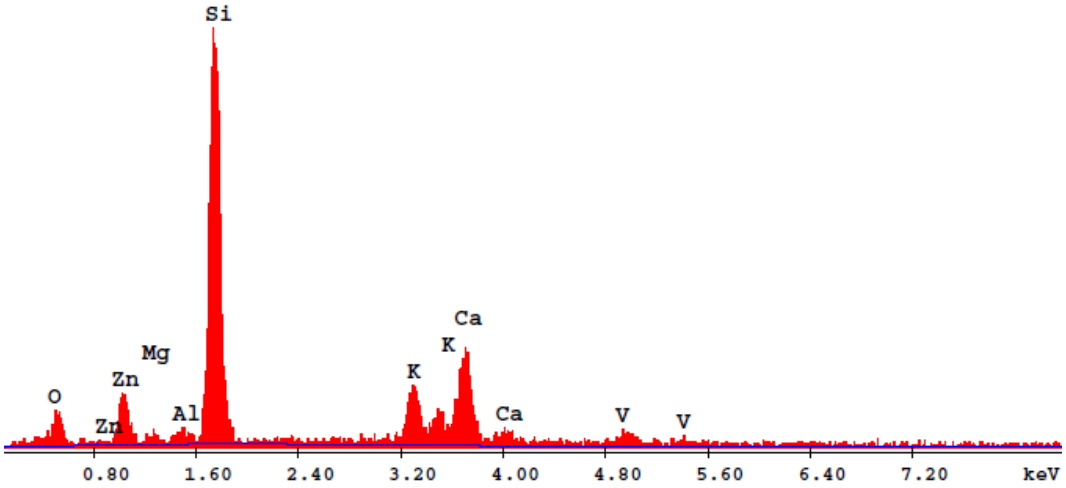

Figure A.4: EDX analysis of ZnO thin film sample electrodeposited at room temperature and dip coated with aqueous solution of NH_4VO_3

Table A.4: EDX quantification table of ZnO thin film sample electrodeposited at room temperature and dip coated with aqueous solution of NH_4VO_3

Element	Wt %	At %
O	23.34	37.84
Mg	1.81	1.93
Al	1.74	1.68
Si	45.21	41.76
K	7.66	5.08
Ca	13.65	8.83
V	2.40	1.22
Zn	4.19	1.66
Total	100.00	100.00

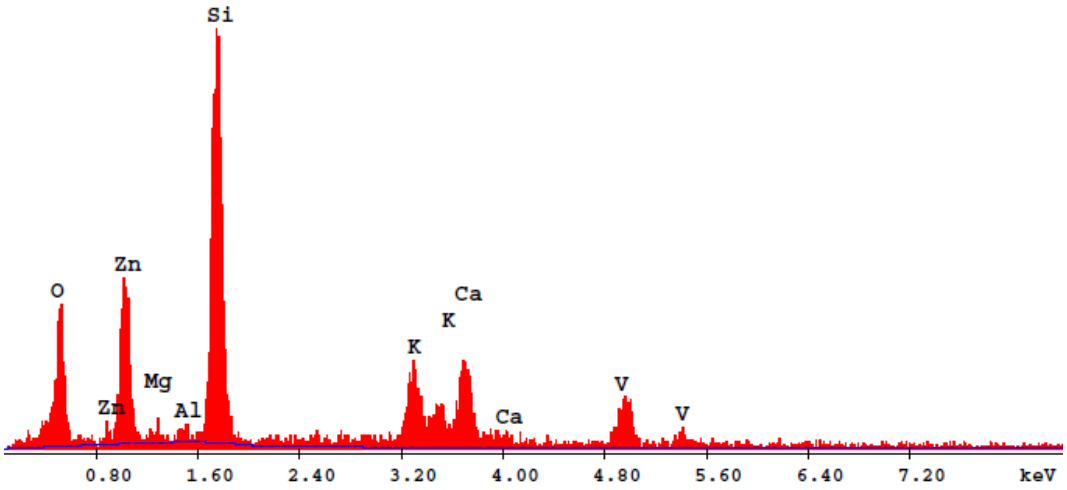

Figure A.5: EDX analysis of ZnO thin film sample electrodeposited at 70 °C and dip coated with aqueous solution of NH_4VO_3

Table A.5: EDX quantification table of ZnO thin film sample electrodeposited at 70 °C and dip coated with aqueous solution of NH_4VO_3

Element	Wt %	At %
O	40.94	59.93
Mg	1.53	1.48
Al	1.21	1.05
Si	29.37	24.49
K	5.57	3.34
Ca	6.66	3.89
V	5.32	2.44
Zn	9.40	3.37
Total	100.00	100.00

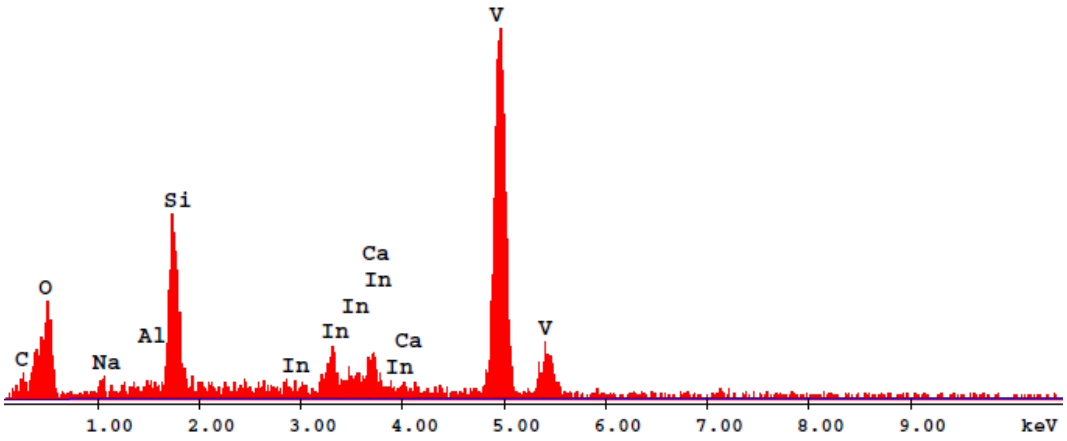

Figure A.6: EDX analysis of ZnO thin film sample electrodeposited at 70 °C and dip coated NH_4VO_3 solution dissolved in oxalic acid

Table A.6: EDX quantification table of ZnO thin film sample electrodeposited at 70 °C and dip coated with NH_4VO_3 solution dissolved in oxalic acid

Element	Wt %	At %
C	13.37	24.83
O	34.33	47.86
Na	2.62	2.54
Al	1.14	0.94
Si	10.38	8.25
In	5.68	1.10
Ca	2.16	1.20
V	30.32	13.28
Total	100.00	100.00

APPENDIX B

AFM IMAGES and CALCULATED AVERAGE AREA ROUGHNESS VALUES of ZNO and VANADIUM DOPED ZNO THIN FILM SAMPLES

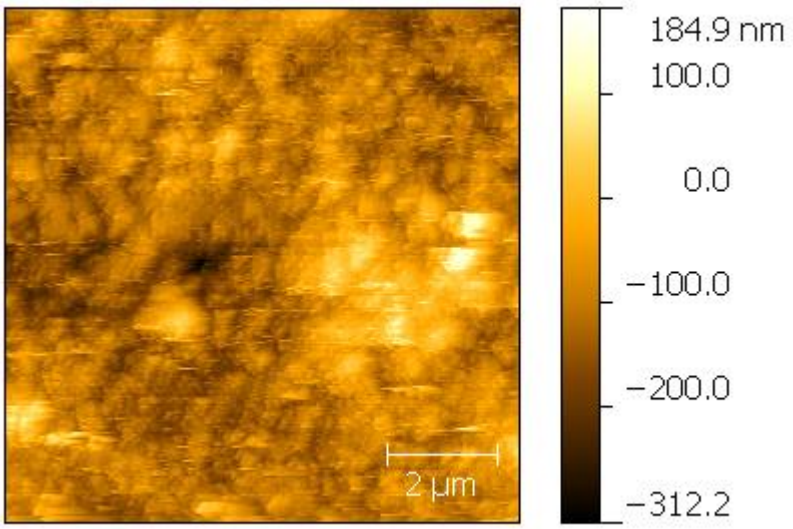

Figure B.1: AFM image of ZnO thin film sample electrodeposited at room temperature

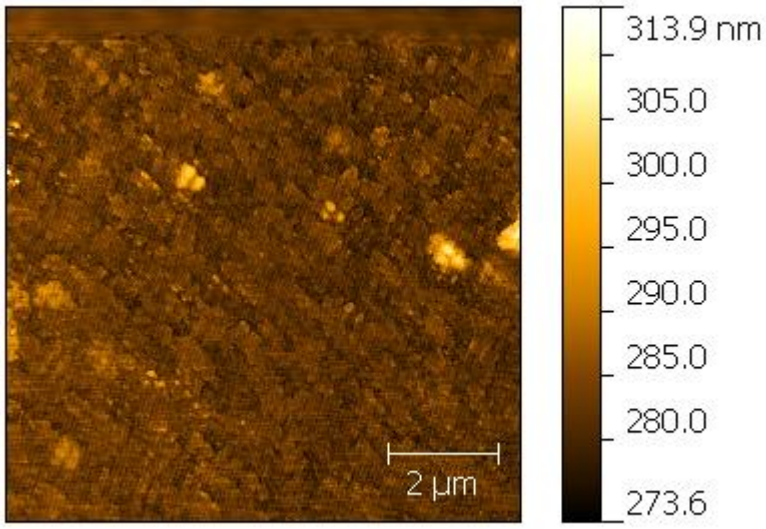

Figure B.2: AFM image of ZnO thin film sample electrodeposited at room temperature and dip coated with aqueous solution of NH_4VO_3

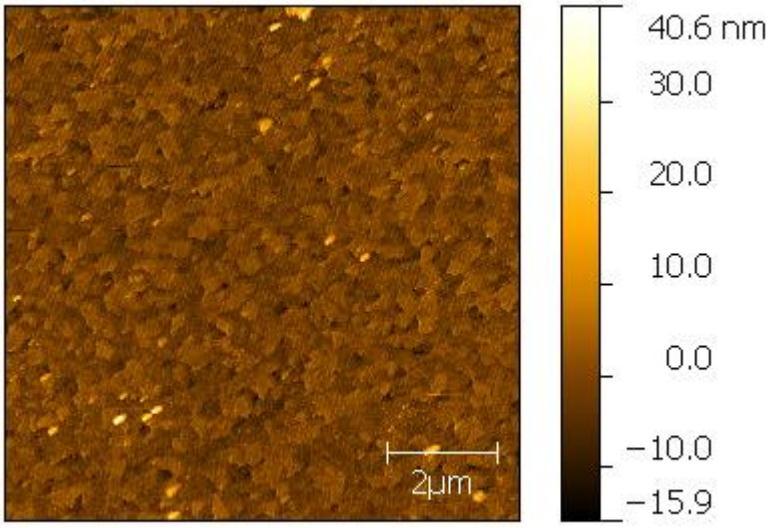

Figure B.3: AFM image of the sample electrodeposited at room temperature and dip coated with NH_4VO_3 solution dissolved in oxalic acid

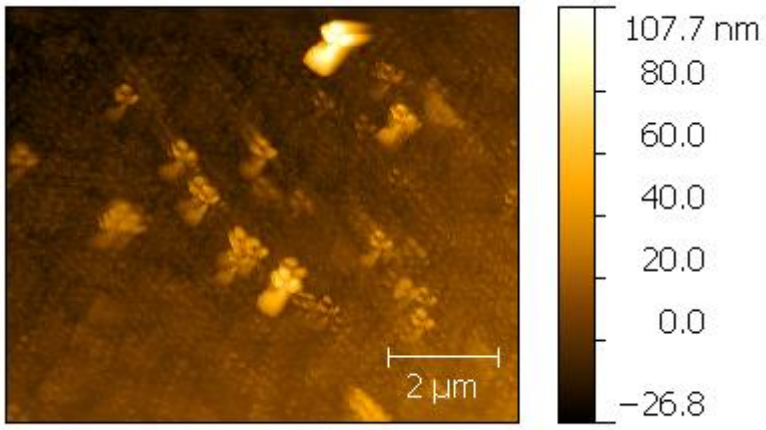

Figure B.4: AFM image of ZnO thin film sample electrodeposited at 70 °C and dip coated with aqueous solution of NH_4VO_3

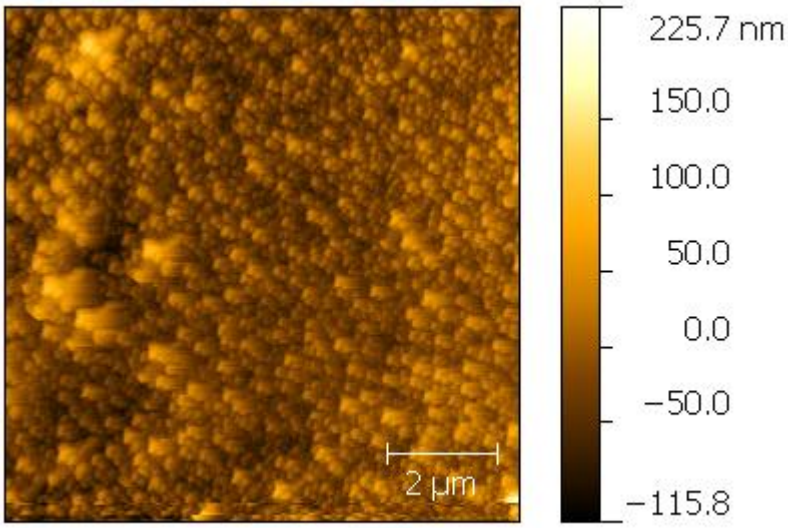

Figure B.5: AFM image of ZnO thin film sample electrodeposited at 70 °C and dip coated with NH_4VO_3 solution dissolved in oxalic acid

Table B.1: Calculated average area roughness values of ZnO and V/ZnO thin film samples prepared at room temperature and 70 °C

Sample	Average Area Roughness (S_a)
ZnO, room temperature	$18.608\ nm$
V^{+5}/ZnO, room temperature	$36.184\ nm$
V^{+4}/ZnO, room temperature	$2.496\ nm$
V^{+5}/ZnO, 70 °C	$4.6926\ nm$
V^{+4} / ZnO, 70 °C	$22.349\ nm$